

Topology Optimized Hemispherical Shell under Asymmetric Loads

by
Grace Melcher

B.S. in Civil and Environmental Engineering
Massachusetts Institute of Technology, 2019

Submitted to the Department of Civil and Environmental Engineering
in Partial Fulfillment of the Requirements for the degree of

MASTER OF ENGINEERING IN CIVIL AND ENVIRONMENTAL ENGINEERING

at the

MASSACHUSETTS INSTITUTE OF TECHNOLOGY

May 2020

©2020 Grace E Melcher. All rights reserved.

The author hereby grants to MIT permission to reproduce and to distribute publicly paper and electronic copies of this thesis document in whole or in part in any medium now known or hereafter created.

Signature of Author:

Grace Melcher
Department of Civil and Environmental Engineering
May 8, 2020

Certified by:

John Ochsendorf
Class of 1942 Professor of Civil and Environmental Engineering and Architecture
Thesis Co-Supervisor

Certified by:

Josephine Carstensen
Assistant Professor of Civil and Environmental Engineering
Thesis Co-Supervisor

Accepted by:

Colette L. Heald
Professor of Civil and Environmental Engineering
Chair, Graduate Program Committee

Topology Optimized Hemispherical Shell under Asymmetric Loads

by
Grace Melcher

Submitted to the Department of Civil and Environmental Engineering on May 8, 2020 in Partial Fulfillment of the Requirements for the Degree of Master of Engineering in Civil and Environment Engineering

ABSTRACT

Domes are an efficient way to span long distances and resist gravity loads. The two kinds of classical domes prevalent in architecture are continuous shells and grid shells. Continuous shells are monolithic concrete or masonry; grid shells reorient material in lattice members to create depth throughout the shell thickness.

This thesis considers the design of a topology optimized hemisphere, a hemispherical continuous shell, and a hemispherical grid shell, and compares the structural performance of these three shells under asymmetric loads. First, a novel topology optimized dome is defined and generated with the objective to minimize strain energy. Then a numerical study is conducted on the three shells, continuous, grid, and optimized hemisphere, to investigate the different structural behavior of each material design scheme. This includes a linear elastic finite element analysis of each hemisphere's response under its own buckling load. Finally, plastic analyses are presented including the effects of large deformations and material yielding to determine the optimized hemisphere's response in comparison to the classical hemispheres. The proposed method uses topology optimization over the new domain of a thin shell lofted into space, as opposed to the more common planar and three-dimensional spaces for structural optimization. This thesis demonstrates good correlation of load capacity between Timoshenko's theoretical predictions and numerical analysis using Abaqus. The proposed topology optimized hemisphere has a seven-fold increase in load capacity under asymmetrical loading, when compared to a grid shell of the same volume.

Thesis Co-Supervisor: Josephine Carstensen
Titles: Assistant Professor of Civil and Environmental Engineering

Thesis Co-Supervisor: John Ochsendorf
Titles: Class of 1942 Professor of Civil and Environmental Engineering and Architecture

ACKNOWLEDGMENTS

This thesis would not have been possible without the thoughtful guidance of my two advisors, John Ochsendorf and Josephine Carstensen. First, thank you John for showing me the immense beauty of the structural world around us. I first developed a love of structural art in your Design of Structures class my sophomore year. It was my favorite class during my 5-year career at MIT. Thank you for advising me from all the way across the Atlantic Ocean even through a global crisis. I cannot thank you enough for generously taking the time to discuss mechanics, point me in the right direction, and for teaching me to value my own work. Thank you for your understanding during the Coronavirus when I needed time to focus on saying my goodbyes to my community on campus and pack up my life at MIT.

Thank you Josephine for helping me pick up the pieces when COVID hit and I had to completely re-think this entire thesis when experiments were no longer possible and I had to move entirely to numerical methods. I truly could not have completed it without your countless hours of guidance in using the software tools and understanding the mathematics behind it all. You taught me that the simplest terms to explain complex concepts are often the most effective. You taught me that academia can be simultaneously approachable, and high quality. Thank you for always challenging me and teaching me to never give up when life gets frustrating. Thank you for the weekly zoom meetings with all your advisees simply to make sure we were doing okay. You have taught me that kindness is a powerful motivating force.

Thank you to my incredible math teachers throughout my learning journey. Deborah Mifflin, you are lovingly remembered, thank you for showing me that math is an infinite puzzle that God built for us to solve. Mrs. McLinda and Mrs. Allen, thank you for letting me be the weird math kid. Sarah Wesley, thank you for teaching me that math is a language, which describes the physical world and showing me *how* to learn well. Mrs. Gajda, thank you for teaching me that men are not better at math than women. Thank you, professors Franz Ulm, Caitlin Mueller, and Tal Cohen, for showing me how to derive and appreciate the incredible forces moving through every seemingly simple structure around us.

Thank you to my MIT Varsity Crew teammates for pushing me harder than I ever thought physically possible. You taught me without pain there is no gain, and with your friendship, you taught me how to endure. Thank you to my classmates Eric Wong and Christine Langston for being my Course 1 companions. I'll never forget the group projects, helping each other learn, and the late night psets. Thank you to my classmates who helped revise this thesis, Eric Wong, Jon Fakkema, and Ellie Brewer.

Finally thank you to my family for giving me the best education and always pushing me to achieve. To Mom and Dad and my brothers Jack and Andrew, thank you all for your service to our country, from the time I was born you taught me that some things are worth immense sacrifice. Thank you Dad for teaching me the difference between radius and diameter as a graduate student, and teaching me a good handshake. You showed me that respect must be earned. Thank you Mom, your career as a pilot in the navy taught Charlotte and me that glass ceilings are just asking to be shattered. Thank you to all of my aunts and uncles who took care of Charlotte and me, the many times that Mom and Dad were deployed and showed me the joy in family, Micky, Bridget, Jen, Cathy, Pat, Sue, and the rest of my massive family. Thank you Charlotte for entertaining my shenanigans and hypotheticals throughout our childhood and for still lifting me up when I need it – I love all of you more than words can express.

Table of Contents

ABSTRACT	3
ACKNOWLEDGMENTS	5
1 INTRODUCTION	8
1.1 Definitions	8
1.2 Background	9
1.2.1 Continuous shells	9
1.2.2 Grid Shells	9
1.3 Motivation	10
1.4 Problem Statement	11
1.5 Approach	11
2 LITERATURE REVIEW	12
2.1 Continuous Shells	12
2.2 Grid Shells	16
2.3 Topology Optimization	17
3 METHODOLOGY	19
3.1 Tools	19
3.2 Continuous Geometry	19
3.2.1 Part	20
3.2.2 Material	20
3.2.3 Property	22
3.2.4 Mesh	22
3.2.5 Assembly and Step	22
3.2.6 Loads and Boundary Conditions	23
3.2.7 Job (Buckling and Static)	23
3.3 Mesh Convergence	23
3.4 Grid Shell Geometry	24
3.5 Optimized Topology	25
3.6 Analyses	28
3.6.1 Primary Analyses	29
3.6.2 Secondary Analyses	30
4 RESULTS	31

4.1	Topology Optimization Results	31
4.2	Buckling Load Validation	33
4.2.1	Symmetric Buckling Load Validation.....	33
4.2.2	Asymmetric Buckling Load Comparison.....	35
4.3	Simple Analysis Results	36
4.3.1	Elastic Stress Results	36
4.4	Yielding and Large Deformation Results	37
4.4.1	Plastic and Nonlinear Geometry Effects	38
4.4.2	Local vs global behavior	40
5	CONTRIBUTIONS AND FUTURE WORK	43
5.1	Novel Achievements	43
5.2	Shell Module for other loads.....	44
5.3	Discussion.....	45
5.3.1	Optimization: Maximizing Buckling Load	45
5.3.2	Potential for Experimentation	45
5.3.3	Effects of Anisotropy.....	46
	Appendix A	47
6	BIBLIOGRAPHY	48

1 INTRODUCTION

The objective of this work is to topologically optimize material distribution in a hemispherical shell and to evaluate the performance of that optimized hemisphere against a continuous hemispherical shell and a hemispherical grid shell. An optimization is conducted by placing an asymmetric load on a hemisphere and specifying an objective to minimize deflection. Then a study is conducted by asymmetrically loading a hemispherical continuous shell, a hemispherical grid shell, and the topology optimized shell and calculating the load/deformation behavior using numerical methods.

1.1 Definitions

This section presents the definitions that will be commonly used throughout this thesis.

Shell structures – a three dimensional curved solid characterized by a very small thickness compared to the other two dimensions, with typical t/R ratios of less than $1/100^{\text{th}}$.

Dome – a rounded vault forming the roof of a building or structure.

FEA – Finite Element Analysis, a simulation of a physical phenomenon using a numerical mathematic technique that discretizes a part into small finite parts and analyzes those pieces rather than the whole solid.

Continuous shell – a monolithic shell structure.

Grid shell – a curved shell structure that is constructed of a lattice, where the forces are concentrated into the members of the lattice, defined by panel size, panel shape, and member cross section.

Optimized shell – in the case of this thesis, an optimized shell is similar to a continuous shell except material has been reoriented using topology optimization.

Topology Optimization – a method that uses FEA to place material efficiently within a domain under loads and constraints, to minimize or maximize some performance metric called the objective.

Meridian Arch – longitudinal arches around the body of a dome, described in Figure 1.1.

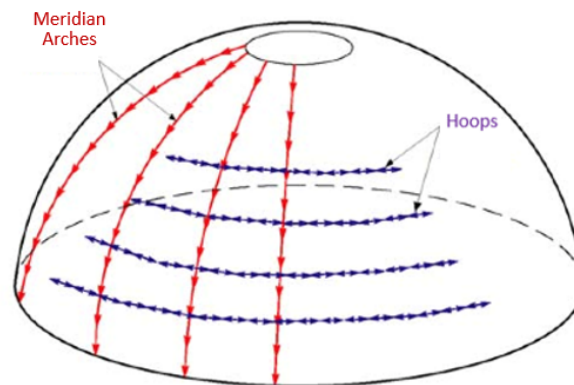


Figure 1.1 – Example dome with meridian arches and hoop members ("Image058," n.d.)

1.2 Background

1.2.1 Continuous shells

Throughout history, the dome has evolved in both engineering and architectural contexts and are among the most prevalent form of continuous shells. These shells are either built with masonry as in ancient times or poured with concrete towards the mid-20th century. The main advancement of the structural shell up until the 21st century was to push them thinner and to span further. Modern era concrete shells often achieve eggshell thinness if their geometry is designed strictly in line with engineering principles. The vast field of modern research on shell structures explores different geometries than a sphere to achieve similar spans and beauty (Otto & Rasch, 1996; Vaulot, 2016). This kind of geometry optimization is called form-finding. Despite their efficiency, due to their thinness and funicular form found geometry relying on gravity loads, a common problem with these shells is buckling under asymmetric load scenarios. This thesis is not a form finding thesis, but rather explores what happens when material in a shell is redistributed and then is asymmetrically loaded.

1.2.2 Grid Shells

With the advancement of prefabricated custom joints, the rise in price of labor, and the preference for natural light, the design field has shifted away from monolithic shells towards grid shells. The quintessential grid shell hemisphere is a geodesic dome. These domes are based on geodesic polyhedrons and were made popular by Buckminster Fuller beginning in 1948 (Borezo & Fuller, 2010). They became very popular due to their ease of transport and constructability, and the design of grid shells largely did

not stray from the geodesic dome until construction methods advanced enough to build irregular reticulated lattices. While these grid shells architecturally improve the spaces with natural light as opposed to continuous shells, they are still susceptible to buckling failure. Much like continuous shells, most of existing literature on grid shells relates to form-finding geometry to maximize bending capacity (Adriaenssens et al., 2009). This differs from topology optimization in that form finding involves a given shape that is relaxed or stiffened into a structural geometry. Topology optimization on the other hand takes a domain and removes material from that domain and typically leads to geometric results that outperform classic lighter designs. Form finding optimization has been done dozens of times by many structural artists of note like Frei Otto (Otto & Rasch, 1996). Another recent type of geometric optimization investigated general principles for increasing grid shells structural rigidity. Malek's study in 2012 is one of the few studies that answers the question of how to place material within a given domain to improve stiffness. The parameters analyzed were panel density, quad versus triangular configurations, and macroscale corrugation placement (Malek, 2012). In the realm of analytical predictions, studies of spherical caps almost exclusively dominate the literature. While there is some existing literature of asymmetric loads on hemispheres, they use methods like form finding and the study of imperfection effects on buckling rather than using topology optimization as a *means* to resist buckling (Baek & Reis, 2019).

1.3 Motivation

The field lacks numerical analyses of asymmetric load cases on hemispherical shells. This thesis focuses on spherical cap geometries, specifically the hemisphere as it is the simplest possible double curved shape and because spherical caps have been studied many times before (Baek & Reis, 2019; Hutchinson et al., 2017; Reis et al., 2020). Hemispherical caps represent the complex doubly curved geometries present in most shell structures, and yet are analytically simple and the amount of previous research on their mechanics lends them as a reliable case study. The field has a robust history of geometrically optimizing shell structures but lacks the use of newer mathematical techniques to explore material placements effects on failure loads. FEA and topology optimization can now be used to rapidly compute forces flowing through structures without an analytical solution.

1.4 Problem Statement

The topological optimization of shell structures is largely unexplored and requires an improved understanding of optimal material placement effect on structural performance. This thesis will use topology optimization first to create an optimized hemisphere. Then this study will investigate the capacity of the optimized hemisphere against a grid shell dome and a continuous dome subjected to asymmetric loads.

1.5 Approach

The approach is threefold; the first step is to model each hemispherical shell. The continuous shell is modelled with Abaqus, the grid shell is modelled using Rhino and the Grasshopper plugin, and the optimized shell is created using the Tosca optimizer Abaqus plugin (*Abaqus/CAE User's Guide*, 2016; *Rhinoceros User's Guide - Introduction*, n.d.). The second step is an eigenvalue analysis of each shell under the asymmetric load case. Then each shell is statically loaded under its own buckling load using only elastic material information and failure mode is evaluated if it can be determined from these two primary analyses. Finally, a nonlinear plastic analysis using the effects of large deformations and yielding behavior will determine load/displacement results. The approach is described below in the flow chart Figure 1.2.

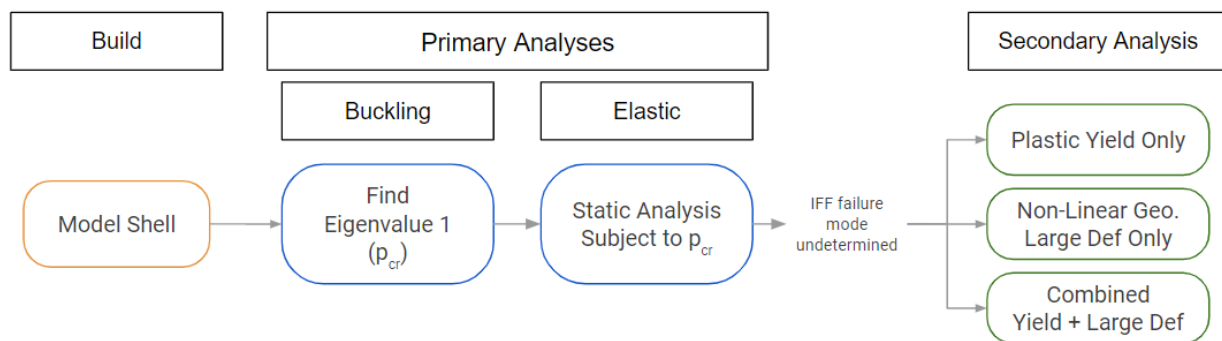


Figure 1.2 – Flow chart describing basic research approach

2 LITERATURE REVIEW

This section presents the existing history and research on shell structures. While shells have high stiffness, the major limiting factor of building these structures is that their rigidity is governed by geometry. This thin geometry leads them to be susceptible to buckling, especially under asymmetric load cases (Timoshenko & Gere, 1961). While there is existing research into form-finding geometry of both the classic continuous and grid shells to increase strength, there is very little investigation into the placement of material within the domain (Baek & Reis, 2019; Otto & Rasch, 1996; Vaulot, 2016). The shell industry would greatly benefit from exploring optimized material placement as a step of the design phase, rather than material placement being confined only to adjustments of grid shell parameters. This literature review will serve as an exploration of existing research into continuous shell forms, grid shells forms, and topology optimization.

2.1 Continuous Shells

The first shell structures were spherical cap domes. The dome geometry dominated the field of shell structures until the mid-20th century, and material types ranged from saplings covered with thatch, to the eventual brick and mortar (Mainstone, 1975). Domes date all the way back to the Neolithic period in the ancient near east where small domes topped squat round houses. The use of the dome shape was ubiquitous among almost all cultures for centuries before any lasting structures were built (Smith, 1971). Since then many more domes have been built, including the impressive Pantheon (115 AD) (first monolithic concrete shell), the Hagia Sophia (535 AD), and St Peters Basilica (1506) as shown in Figure 2.1.



*Figure 2.1 – The Pantheon, The Hagia Sophia, and St. Peter's Basilica
(Hagia Sophia, n.d.; St. Peter's Basilica, 2019; The Pantheon, n.d.)*

After the mid-20th century the popularity of concrete combined with cheap labor drove the advent of monolithic concrete shells (Kovářík et al., 2019). Felix Candela is widely regarded as a pioneer of building these shells. In the 50s and 60s, he built dozens of shells through his architecture firm in Mexico. Shells

became very in-vogue and architects like Eero Saarinen built Kresge Auditorium at MIT in 1955, which is $1/8^{\text{th}}$ of a spherical shell supported on three points. However, this was not a geometrically efficient shape to carry loads as the thrust lines are not resolved. The failure of this structure reflects the very narrow engineering principles that shell structures must obey. Ultimately the structure needed major overhaul and reinforcements after construction due to larger than anticipated deflections in the perimeter beams. Instead of a three point supported shell, the $1/8$ sphere is now supported along its entire perimeter by vertical mullions cleverly hidden behind the glass curtain wall as shown in Figure 2.2 (AD Classics, 2014). This proved that while shells can be very efficient as in Candela's designs shown in Figure 2.3, there is still much that the field does not theoretically understand about shell behavior.



Figure 2.2 - Kresge Auditorium (Foxe, 2010)

In the early 20th century, investigations into analytical solutions for stresses and displacements, specifically of spherical cap domes, became very popular. And during that period the research focused on the principles of concrete shell design (Molke & Kalinka, 1938). These solutions were primarily studying shallow spheres, although in 1919 Germany, E. Schwerin investigated a hemisphere dome and developed a solution for symmetric loading “by combining membrane stress analysis with the edge effects solution” (Berman, 1946; Reissner, 1946). The hemisphere shell is the epitome of a steep dome and throughout the analytical research it was found that domes with a lower span/height ratio are governed by bending through the thickness of the shell, and shallow shells with a higher span/height ratio are governed by membrane forces through the span of the shell (Timoshenko & Gere, 1961). Most sphere caps that were analytically solved in the early 20th century were symmetric loading cases. The few that investigated asymmetric loads did so with a pressure load over half of a sphere (Meissner, 1915; Schwerin, 1919).

Many other analyses at the time focused on boundary conditions and edge effects rather than different particular loading scenarios (Geckeler, 1926; Pasternak, 1926). These studies focused on predicting stresses and critical loads, but none investigate the question of where to place material.



Figure 2.3 - Felix Candela's L'Oceanogràfic and Palmira Chapel ("L'Oceanogràfic," 2020; Palmira Chapel, n.d.)

The recent resurgence of interest drove the rise of experimental and numerical investigations into critical buckling loads of spherical caps. These studies build on Timoshenko's well established critical buckling load equation shown in equation 2.1 (Timoshenko & Gere, 1961). Where E is the Young's Modulus, ν is the Poisson's ratio, t is the thickness, and R is the radius of the spherical cap.

$$p_{cr} = \frac{2E}{\sqrt{3(1-\nu^2)}} \left(\frac{t_{eq}}{R} \right)^2 \quad (2.1)$$

Many of these new studies specifically investigate the effects of imperfections on the critical buckling load (Al-Rashed et al., 2017). They are similar to earlier analytical studies in that the goal was to predict the buckling load. Loads are commonly either applied at the pole in a point load as in Reis's study on the indentation deformation patterns of elastic shells, or as a pressure load over some portion of the hemisphere (Hutchinson et al., 2017; Nasto & Reis, 2014). One particular study that investigated the buckling load of hemispheres studied the effect of through-thickness defects on what is defined as an experimental "knockdown effect" (Reis et al., 2020). This knockdown effect is described as the difference between the Timoshenko's derived buckling capacity solution and experimentally found buckling loads.

Though an analytical solution has not been developed for asymmetrically loaded spheres, there have been experimental and numerical investigations into asymmetric loading effects. One study conducted by Hutchinson investigated the effect of an off center indentation imperfection on the critical buckling load of a hemisphere (Hutchinson et al., 2017). This study investigated the effects of a shell imperfection on

the critical buckling load when probed from different angles relative to the pole (Hutchinson et al., 2017). Another study investigates lateral loading on masonry domes, which is a kind of asymmetric load. This study applied a static lateral load by tipping the dome and determined collapse load (DeJong, 2009). Yamada and Yamada developed a unique *numerical* solution for a pressure load distributed over half of a spherical cap. Both the Timoshenko and the Yamada solutions are derived for shallow spherical caps, however their boundary conditions differ slightly as depicted in Figure 2.4 (Timoshenko & Gere, 1961; Yamada & Yamada, 1985). The Yamada solution defines a new shallowness parameter $\lambda = \sqrt[4]{12(1 - \nu^2)} \frac{a}{\sqrt{Rt}}$ to describe the assumptions of the solution $6 \leq \lambda \leq 15$. Yamada found that under an asymmetric load condition, the critical buckling load lies 17-30% lower than Timoshenko's symmetric solution (Yamada & Yamada, 1985). This metric will be used to validate FEA results in chapter 4.

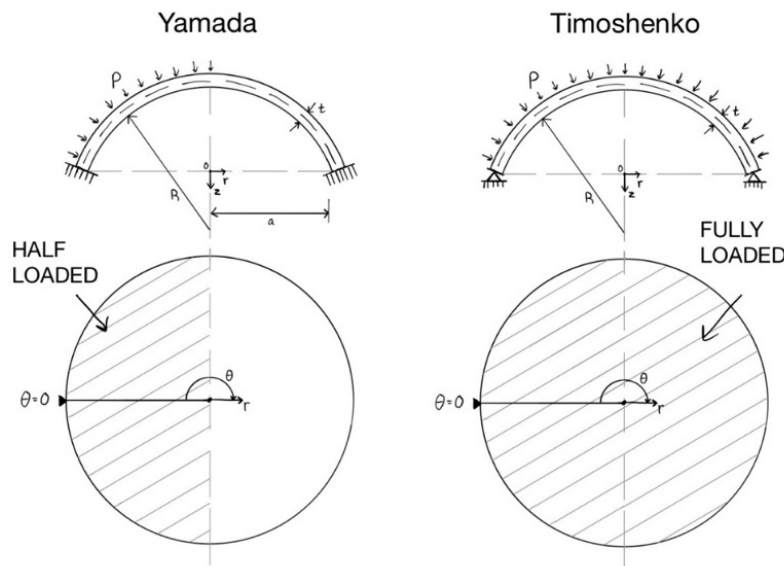


Figure 2.4 - Timoshenko vs Yamada's boundary condition and loading assumptions for their respective buckling load solutions

Through the past century, literature has shifted from deriving analytical stress solutions towards predicting and increasing buckling loads with numerical and experimental processes. However, there are few investigations into exploring placement of material to achieve these goals. Grid shells open the discussion of arranging material, both geometrically and parametrically with panel dimensions, but the scope of grid shells is limited to reticulated forms, and do not topologically optimize placement of material.

2.2 Grid Shells

Grid shell structures were first made popular by Buckminster Fuller starting in 1948 with his geodesic dome (Borezo & Fuller, 2010). Up until the 1970s, grid shells largely remained within the scope of the geodesic dome. In the 1990s and 2000s, grid shells experienced a resurgence in interest due to improved construction methods using digital fabrication (Mesnil et al., 2015). By this point Timoshenko's spherical cap numerical solution could be used to validate FEA processes, which could then be used to investigate forces in grid shells. The early 2000s brought about numerical studies of coupled instabilities, rigidity of joints, and the effects of imperfections on critical failure loads (Bălut & Gioncu, 2000; Gioncu, 1995)(López et al., 2007). The questions that needed answering became "what is the optimal span to height ratio?" and "how does the size and shape of grid panels affect performance?" (Malek, 2012). Malek conducted a thorough parametric study of real design parameters such as shell height, panel shape, and panel size on load bearing capacities (Malek, 2012).



Figure 2.5 - The Great Court at the British National Museum, Smithsonian National Museum, Japan Pavilion ("Great Court," 2016; Japan Pavilion, Hannover Expo 2000, n.d.; Smithsonian American Art Museum, n.d.)

On the theoretical side of the research, predicting the buckling capacity of spherical grid shells requires approximating its "equivalent thickness" t_{eq} and using Timoshenko's buckling equation. Some of the approximation methods that have been used are as follows: equivalent volume, equivalent stiffness, or orthotropic equivalence (Wright, 1966) (Kollár & Dulácska, 1984). Despite their obvious differences from continuous shells, the well-established dominant failure mode for reticulated shells is buckling (Gioncu, 1985). Therefore, studies by mechanists focused on what influences the buckling load, much like the more recent investigations into continuous spherical caps (Lefevre et al., 2015). There is a huge body of research dedicated to form finding grid shells to resist buckling instability much like continuous shells (Mesnil & Engineering, 2013; Paoli, 2007; Vulot, 2016). This resurgence also inspired some investigations into asymmetric loading as in the Reis study which investigates hemispherical elastic grid shells under point load indentation (Baek & Reis, 2019). This involved periodically indenting a highly elastic grid shell

to record rigidity at each point. Still there has been no investigation into answering the question of *where to place material to mitigate critical buckling under asymmetric loads*.

2.3 Topology Optimization

Topology optimization uses a mathematical method to solve a formal optimization problem. Practically it uses FEA to place material efficiently within a domain under given loads and constraints, to minimize or maximize some performance metric called the objective. For example in a very basic 2D optimization the design variable is the density of each meshed element in an FEA model and the objective is to minimize strain energy. The FEA essentially solves for the strain in each element as a result of some load and then finds local or global minima of the total strain energy by changing the design variable (density function) (M. Bendsøe, 1989). As it is an iterative process and relies on computational power, it is a relatively new method with some of the first studies beginning in the late 80s. Topology optimization has been used in a number of different fields including mechanical, medical, and structural. Some examples include maximizing the stiffness of ear prosthetics, beams, truss structures, and plates (Martin P. Bendsøe & Sigmund, 2003; Milazzo et al., 2020). The 1998 Bendsøe study depicted in Figure 2.6 shows the optimization of material placement in a 2D domain.

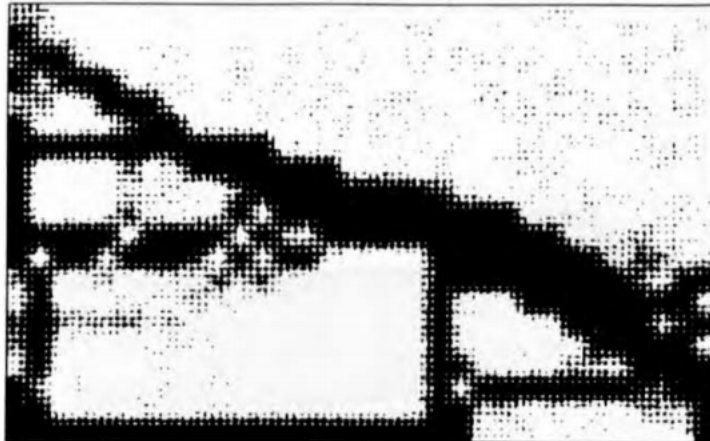


Figure 3.6 - Topology optimization of 2D domain using homogenization method, 36% volume result. Black indicates material placement, white indicates void. Load was placed on the bottom right corner with pins on the left side of the domain (Martin Philip Bendsøe & Kikuchi, 1988)

Topology optimization only outputs results that take into account the constraints that the user inputs. In this way it can be sensitive to user choices and how well the problem is defined. There are not many studies that investigate topology optimization on a structural scale. Some examples of structural scale studies include investigations of pattern gradation for the conceptual design of buildings, and

topology optimization for supertall braced frames (Stromberg et al., 2011, 2012). Most topological optimization studies in the structural engineering field have focused on minimizing compliance (Vantighem et al., 2020). Interest in directly maximizing the buckling load has only surfaced in the last few years (Ferrari & Sigmund, 2019). This study was among the first of its kind because eigenfrequency is notoriously erratic and rarely converges due to its high sensitivity (Bruyneel et al., 2008). Sigmund and Ferrari successfully completed their optimization by investigating the effect of different lower bound compliance constraints on their implementation. However, in order to achieve this they used non-conforming finite elements, inconsistent sensitivities, and replaced single value eigenvalue constraints with an aggregated measure (Ferrari & Sigmund, 2019). These measures were outside the scope of this thesis. Since bending is the well-established failure mode of shells and is the impetus for buckling, this thesis will use the classical method of maximizing stiffness and investigate both deformations and buckling capacity in the results. Topology optimization in the field of shells is sparse and consists of combinations of optimizing shape and topology, but primarily the focus is the simultaneous combination of these methods on shallow abstract shapes under *symmetric* loading conditions (Hassani et al., 2013; Xia et al., 2019). This thesis rather, provides a topology optimization on the more steeply curved dome, uses asymmetric loading conditions, and controls the volume constraint for practical application and comparison against classic domes.

Ultimately the field of hemispherical shells is robust in its analytical analyses of critical pressure buckling loads and numerical form finding methods. However, there is less research on asymmetric loading effects on shell behavior and no studies on optimal material placement in dome geometries. While form-finding methods are useful for creating abstract funicular geometries, there has been little investigation into where to directly place material to stiffen shells. While topology optimization is a versatile tool used in many industries, it has not been used to place material effectively in shells specifically to investigate these buckling loads. This thesis will investigate both the use of topology optimization over a hemisphere domain, and that optimized shapes performance compared to the classical dome geometries.

3 METHODOLOGY

This thesis goals are to calculate the load bearing capacity and failure behavior of a continuous shell, grid shell, and optimized shell. This is achieved in a three-step process; computationally build the three different hemisphere geometries, conduct buckling and elastic stress analyses under each geometries' buckling load, and conduct plastic analyses including nonlinear geometry effects and yielding behavior. This chapter presents the methodology used to answer the following questions:

- Can topology optimization be used to optimize the material placement in a hemisphere?
- Does an optimized hemisphere resist bending and buckling under asymmetric loads better than the classical continuous and grid shell hemisphere geometries?

3.1 Tools

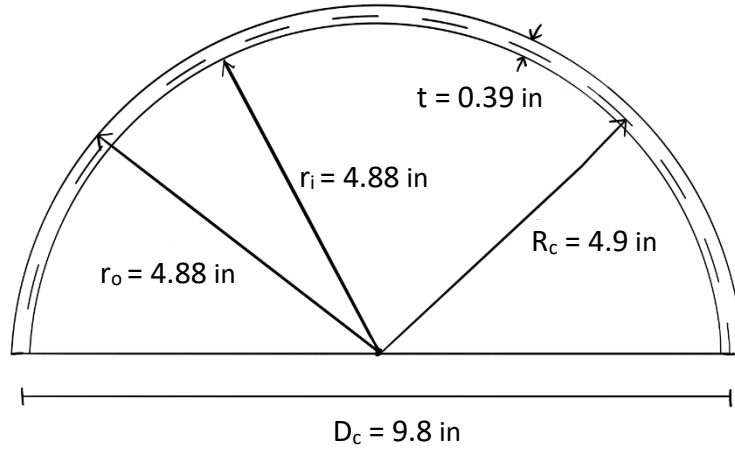
The two tools used to carry out the analysis and topological optimizations of the three respective hemispheres: continuous, grid, and optimized, are Abaqus/Tosca and Rhino/Grasshopper. Abaqus is an FEA software produced by Dassault Systemes (*Abaqus/CAE User's Guide*, 2016). The analysis types that are utilized in this thesis are all implicit, including static linear stress, linear perturbation, and plastic stress analyses. The setup for Abaqus is described in the subsequent section. Rhino is a CAD software with a parametric plug-in called Grasshopper, which is used to create the grid shell geometry as described in Appendix A (*Rhinoceros User's Guide - Introduction*, n.d.). Due to the COVID-19 crisis of 2020, this thesis does not conduct experimental validation but models the three hemispheres assuming experimental limits so that future experiments can be conducted based on this work. The constraints defined in the respective software are based on experimental assumptions for a Stratasys F170 FDM printer such as print bed limits, thickness limits, and physical load placement constraints.

3.2 Continuous Geometry

This section describes the Abaqus process used to create the continuous shell geometry. Abaqus has different modules and the settings applied in each module to create the hemisphere geometries analyzed in this study are described. It is important to note that Abaqus does not take units as an input, so it is the user's responsibility to ensure uniform units. For the purpose of this thesis, inches and psi are used. To make each of the shells comparable, they all must have equal volume (Malek, 2012; Timoshenko & Gere, 1961). This enables equivalent comparison of their performance, which is discussed in results. The volume

limiting geometry in this case is the continuous shell. Stratasys F170 FDM printer bed limits are 10” and the minimum thickness of a printed ABS wall is 0.039” because any part thinner than that is imperfection prone. The calculations for the volume of the continuous shell are shown below in equation 3.1.

Figure 3.1 – Continuous hemisphere shell dimensions



$$V = \frac{2}{3}\pi(r_o^3 - r_i^3) \quad (3.1)$$

$$V = 5.88 \text{ in}^3$$

This volume is used to construct the grid shell beam profiles discussed in section 3.3, as well as define the material constraint on the optimized shell in section 3.4.

3.2.1 Part

This first module to define the continuous shell geometry is the part module. This is conducted by first creating a sketch of a quarter circle of radius 4.9” and revolving it 360° with “shell-homogeneous” parameters selected.

3.2.2 Material

Once the part is created, material properties are defined in this module. For this thesis, ABS plastic properties are used because there is sufficient literature on isotropic versus printed material properties (Fang, 2017; Kuznetsov et al., 2018; Tam, 2015). The ABS filament specifications published by Stratasys are described below in Table 3.2. Frank Fang at MIT conducted thorough research on the effects of FDM on the material performance of ABS plastic and found that the strength of the printed filament were *lower* than the Stratasys publication suggested (Fang, 2017). Table 3.1 provides the differences between the

Stratasys publication and the findings of that analysis. While the Fang study is thorough and provides a comprehensive analysis, the field's conclusions vary widely on how much the strength of printed filament decreases after printing. For this reason, *this thesis uses the Stratasys published values*. Further discussion of the effects of anisotropy will be discussed in section 5.4. In this study for the primary analyses, using only elastic behavior (discussed in section 3.6), yielding material information is not needed. However, for the secondary analyses, the yielding data of ABS plastic is interpolated from the % strain values published by Stratasys and is tabulated below in Table 3.2.

Table 3.1 – Stratasys published ABS material property values and modification results (Fang, 2017)

Mechanical Properties	Stratasys Value		Test Results				
			Min		Max		Percentage
Ultimate Tensile Strength	4785 psi	33 MPa	1102 psi	7.6 MPa	3002 psi	21 MPa	23-63%
Yield Strength	4495 psi	31 MPa	1088 psi	7.5 MPa	2886 psi	20 MPa	24-64%
Elastic Modulus	319000 psi	2200 MPa	133400 psi	920 MPa	220110 psi	1518 MPa	42-69%
% Strain at Break	6%		0.86%		5.73%		14-96%
% Strain at Yield	2%		0.86%		1.68%		43-84%

Table 3.2 – Yield behavior values of ABS filament

Yield Data		
Yield Stress (psi)	Yield Stress (MPa)	Plastic Strain
4500	31.0	0
4650	32.1	0.01
4750	32.8	0.02
4800	33.1	0.04
1000	6.9	0.05

3.2.3 Property

Thickness of the shell part is defined by specifying a section size in the property module. For an ABS hemisphere of 9.8" diameter, the thickness 0.039" is used. For a "shell" part as defined in section 3.2.1, thickness is offset from the middle surface of the shell. This means half of the specified thickness is offset from the outside face, and half is offset from the inside face of the hemisphere.

3.2.4 Mesh

Mesh convergence must be checked to ensure the FEA is producing accurate results. For the details on the mesh convergence test conducted for this thesis, see section 3.3. As a result of the convergence study, a mesh size of 0.14" is chosen. This is specified for the hemisphere by opening the "seed part" in the mesh module and specifying the "approximate global size" of the mesh elements.

3.2.5 Assembly and Step

The assembly module is where sets of points are defined. These sets are later called in the loads and boundary conditions modules. This thesis analyzes asymmetric loading conditions, so the point sets are chosen to reflect asymmetry. One set is created on the bottom rim of the shell to define boundary conditions. The two-point load set is created by choosing the two points at the center of two adjacent quadrants of the hemisphere.

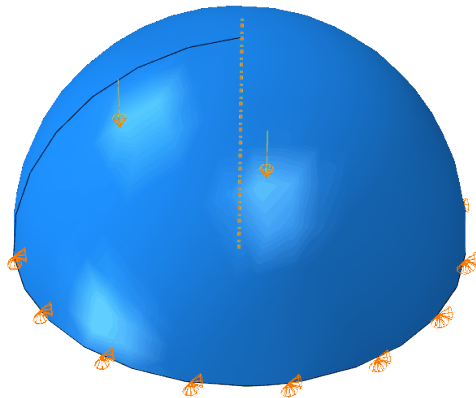


Figure 3.2 – Two asymmetric load points applied to the continuous hemisphere shell Abaqus isometric view

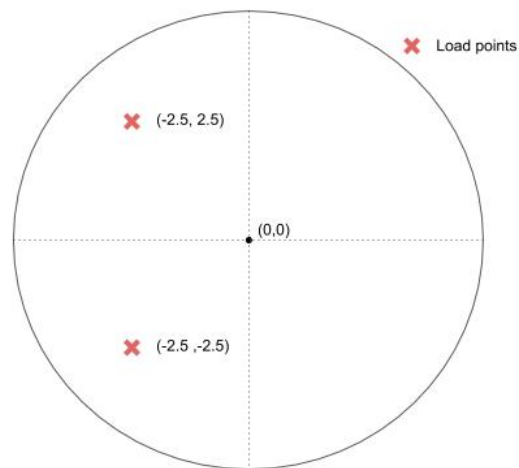


Figure 3.3 – Two asymmetric load points applied to hemisphere's plan drawing

The step module is where the analysis type is defined. For the primary analyses this study used the buckling and static steps respectively to determine both the buckling load p_{cr} of the shell and then

conduct an elastic analysis on the hemisphere. Then only the static step is used for the secondary analyses the hemisphere.

3.2.6 Loads and Boundary Conditions

Continuous pin connections are assumed as the boundary condition around the base rim. This is standard with the analytical literature. Pins constrain all positional displacements and leave the rotational components of the matrix unconstrained. Two loads are created that call the two-point set defined in the assembly module. The first load totaled one pound (0.5lbs on each point) and is used with the buckling step determine the critical buckling load (p_{cr}) of the hemisphere as is standard in FEA eigenvalue analyses. The second load that calls the two-point set is equal to the value of the mode 1 eigenvalue found in the buckling step. This process is described in more detail in section 3.6.

3.2.7 Job (Buckling and Static)

The function of the Job module is to take all the data defined in the previous sections, to run the analysis, and to store the resulting data. A job is created and run to complete the buckling analysis (using the 1lb load) to calculate the lowest eigenvalue. Then a separate job for the static analysis of the continuous hemisphere is created and run with the static step. A summary of model parameters is tabulated below in Table 3.3.

Table 3.3 – Model parameters in both imperial and metric values

Input Value	Imperial	Metric
Diameter (on center)	9.8 in	24.9cm
Thickness	0.039 in	1mm
Volume	5.88 cu in	96.4 cu cm
Mesh size	0.14 in	3.56 mm
Yield Strength	4500 psi	31MPa
Ultimate Strength	4800 psi	33MPa

3.3 Mesh Convergence

Mesh convergence is checked to verify the accuracy of the FEA. For this study a mesh size is chosen in accordance with the computational time tradeoff. Since the objective of the optimized hemisphere is to minimize strain energy (discussed in section 3.5), total strain energy is the metric used to check for monotonic convergence (equation 3.2). This is achieved by running static analysis jobs with a load of

100lbs on the two-point set (and all the other previously defined Abaqus model settings) and refining the mesh size to smaller and smaller values until the strain energy solution converges. The study is conducted by first choosing a large mesh of 0.5" elements in the mesh module, running the analysis, recording the resulting strain energy, slightly refining the mesh size, and repeating this process. The discrete model strain energy is presented below, where d is displacement, K is the stiffness matrix, and Kd is equal to the applied force.

$$E = \frac{1}{2} d^T K d \quad (3.2)$$

As the mesh is refined, the strain energy approaches the reference energy E_{ref} , which is found by the FEA of a very refined mesh. The strain energy is plotted with the computational time to understand a tradeoff. Normally strain energy approaches from below towards convergence at the supremum limit of the reference energy, which is observed in these results shown in Figure 3.4. It is shown that the mesh size of 0.14" is close to the converging strain energy value without sacrificing on computation time. The continuous shell geometry is used to validate the mesh convergence.

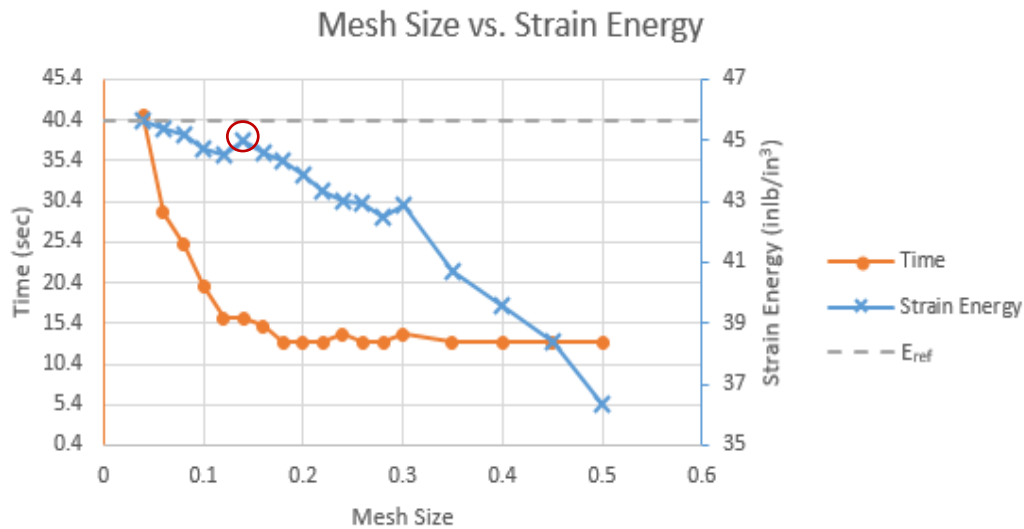


Figure 3.4 – Mesh convergence test data. Conducted using total strain energy plotted with solution convergence time

3.4 Grid Shell Geometry

This section describes the process for building and analyzing the grid shell hemisphere. The Rhino plugin Grasshopper is used to build the grid shell geometry, the code for which is provided in Appendix A. The grid shell is parametrized in grasshopper by the base width, the number of meridian arches, the number of hoops, and the angle of embrace of the sphere. Given the loads placed at the center of two adjacent quadrants it is imperative that a meridian arch and a hoop meet at a joint underneath those two

load points. The grid shell geometry in this thesis has 12 meridian arches, 6 hoops, and a 90° angle of embrace.

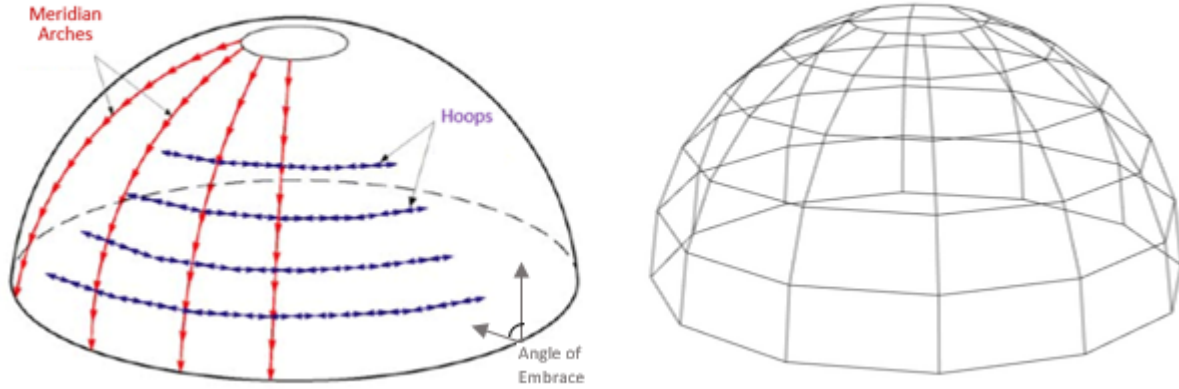


Figure 3.5 – Construction of grid shell hemisphere with parameters meridians, hoops, and angle of embrace

Once the geometry is created in Rhino, it is imported into Abaqus into a separate model as a part. The model setup is completed on the continuous shell as defined in section 3.2 is exactly copied for the grid shell hemisphere. The only difference in Abaqus between the continuous hemisphere model and the grid shell model is the definition of beam members in the grid shell. A beam “profile” is assigned in the property module of the grid shell model and assumed that all joints are fixed. In order to determine the proper section size for the grid shell members, the profile is assigned so that the volume of the grid shell is the same as the volume of the continuous shell. The total sum length of the grid shell members is 207”. The calculation for the beam profile with respect to the volume established by the continuous shell results in a beam profile of 0.17” x 0.17”. Calculations are shown below in equation 3.3.

$$\begin{aligned} V &= L * w^2 & w &= 0.17 \text{ in} \\ V &= 5.88 \text{ in}^3 & L &= 207 \text{ in} \end{aligned} \quad (3.3)$$

3.5 Optimized Topology

This section describes the process for how the topology optimized hemisphere is discovered. Topology optimization is a method that uses FEA to maximize or minimize some performance metric called an objective, by toggling given variables, under given loads and constraints. In the structural industry it is common to minimize compliance (strain energy). By definition this is a minimization of

deflections at points where exterior loads are applied, which frequently corresponds to the locations of the largest deflections. This study also minimizes compliance (deflections) as the objective because in shells, deflection and bending is the impetus for the well-established buckling failure mode. Presumably the minimization of bending in the optimized hemisphere will result in a higher critical buckling load than in the classic continuous and grid shells described in the previous sections. The problem formulation for the optimization conducted in this thesis is given below in equation 3.4. The objective is to minimize compliance by toggling the variable density of each finite element ρ , subject to the inherent equilibrium constraint defined by h , a volume constraint defined by g , and the minimum element density tolerance defined by ρ_{min}^e . The solution of this problem formulation is a new density applied to each finite element in the mesh of the hemisphere, either 0 or 1. This is how the optimizer removes and replaces material within the domain defined by the input mesh. The variables in the problem formulation are as follows, f is the compliance, F is the applied forces, d is the displacements, K is the stiffness matrix, v^e is the element mass, and V is the chosen volume constraint value.

$$\begin{aligned}
& \underset{\rho}{\text{minimize}} && f = F^T d \\
& \text{subject to} && h = K(\rho^e)d - F = 0 \\
& && g = \sum_{e \in \Omega} \rho^e v^e - V \leq 0 \\
& && \rho_{min}^e \leq \rho^e \leq 1 \quad \forall e
\end{aligned} \tag{3.4}$$

Instead of the original interpolation method which allows gradient based optimizers by multiplying the original density stiffness matrix K_0^e of each element simply with ρ^e ...

$$K^e = (\rho^e + \rho_{min}^e)K_0^e \tag{3.5}$$

...the SIMP interpolation method was used to encourage the solution density convergence (M. Bendsøe, 1989). SIMP interpolation multiplies the original element stiffness matrix by its new density to the power of $\eta = 3$ as shown below, followed by the appropriate sensitivity modification:

$$K^e = ((\rho^e)^\eta + \rho_{min}^e)K_0^e = \tilde{\rho}^e K_0^e \tag{3.6}$$

$$\frac{\partial f}{\partial \rho^e} = \frac{\partial f}{\partial \tilde{\rho}^e} \frac{\partial \tilde{\rho}^e}{\partial \rho^e}$$

SIMP was used to encourage solution convergence. This essentially encourages ρ^e either to converge towards 0 or 1, and $\eta = 3$ was chosen because it has been proven to work well (M. P. Bendsøe & Sigmund,

1999). The practical implementation of this problem formulation is done in the Tosca optimizer by defining the objective, constraints, and design responses. To complete this, first a copy of the continuous shell model is created on which to base the optimization. Recall that the beam dimension of the grid shell is 0.17". The section thickness of this new model hemisphere shell is defined as 0.17", so that the optimized shell members have identical thickness as the grid shell. All of the other conditions for this model are the same as the continuous shell except for the thickness. Then the objective, constraints, and SIMP interpolation are defined in the optimization module in Abaqus. First in the optimization module a topology optimization "task" is created. In the advanced section of the task, SIMP material interpolation is selected with a penalty factor of 3. Within that task in order to specify the objective and constraints in Abaqus, two single-term design responses are created. The first is specified as volume, the second as strain-energy. Then an objective function is created and the target specified as a "minimization of design response values" and the strain energy response is assigned. Then a constraint is created and the volume design response is assigned as less than 5.88in³ as discussed in the previous sections. Consider a topologically optimized flat plate with a load applied on the right side as shown in Figure 3.6. Red is density 1 and blue is density 0. Results are expected to look similar to this except instead of a flat plate the results in this study will be a hemisphere; and with much finer resolution.

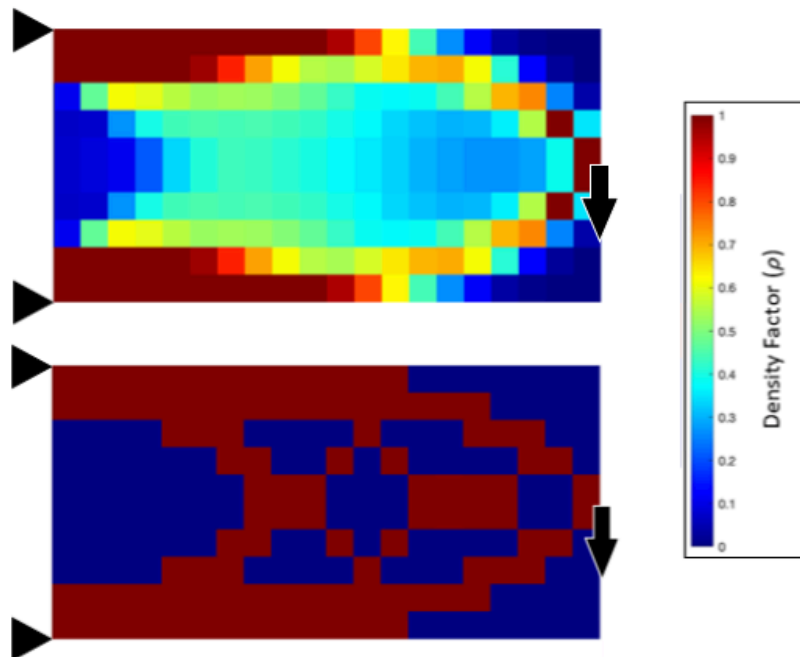


Figure 3.6 – Large mesh plate topology optimization example with boundary conditions and loads. Linear interpolation method (top) and optimization using SIMP interpolation (bottom)

3.6 Analyses

This section describes the process developed to analyze each shells behavior under equal loading conditions. Recall that the purpose of these analyses is to determine each shells failure mode. Whether that is buckling failure or material yielding, the goal is to compare the optimized hemisphere's performance with the classical shells performance.

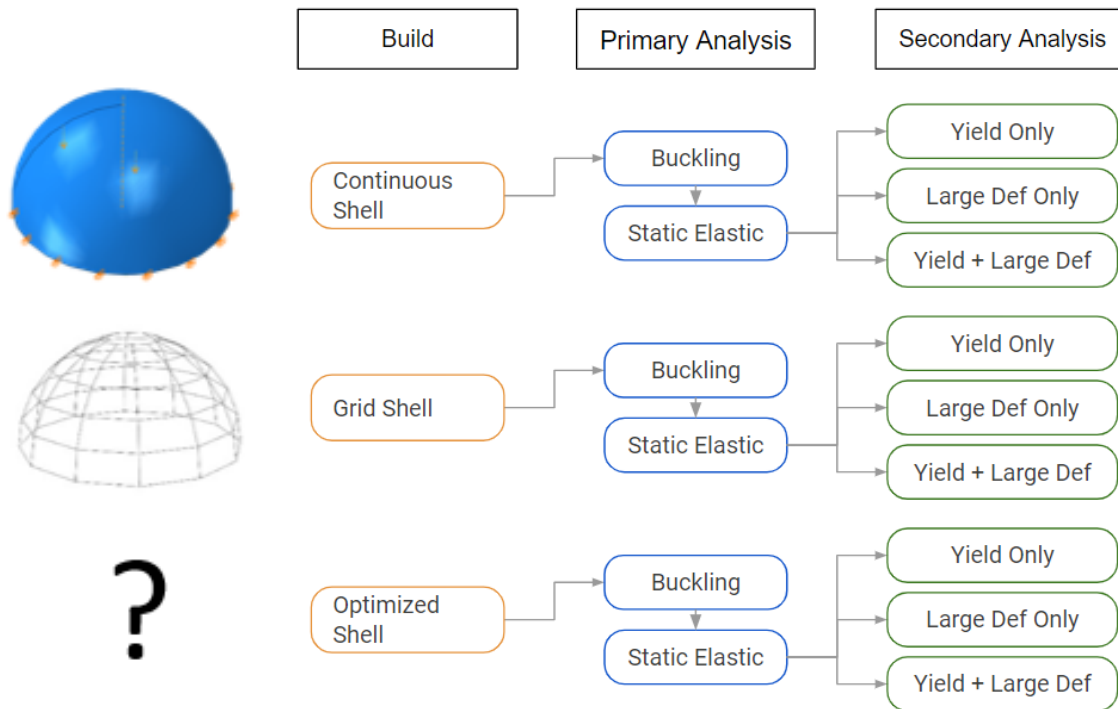


Figure 3.7 - Overview of approach for all three hemisphere shells

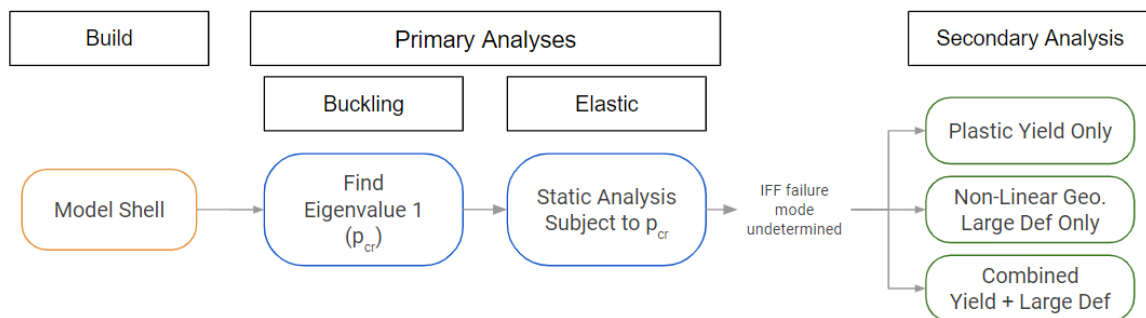


Figure 3.8 - Analysis process for each hemisphere shell

3.6.1 Primary Analyses

The purpose of the eigenvalue and static elastic analysis is to determine if any of the shells fail in buckling. An eigenvalue analysis is conducted first on each of the three shells, using the loads, boundary conditions, etc. described in section 3.2 and the lowest discovered eigenvalue (critical buckling load) p_{cr} is found for each geometry. This analysis is completed first to discover the upper load limit of each shell because a static analysis with only elastic material information has no upper load limit. Without discovering the upper buckling load limit first, results in the stresses simply linearly increasing as a reaction to the users chosen load. Therefore if the buckling load is placed on the shell, and the resulting stresses are lower than the ABS ultimate strength value (4800psi), it is concluded that the part fails in buckling. Local or global buckling is determined by the deformed shape. If the stresses are higher than the materials ultimate strength value in any of the three hemispheres, then further analysis is required using more realistic material behaviors and is completed in the secondary analyses. Once the first eigenvalue (p_{cr}) is found in the buckling step, that load is equally divided into eight to disburse around the two load points for each hemisphere in the subsequent static step shown in Figure 3.9. Placing the load directly on the two original load points results in inaccurate concentration of stresses at those points. Disbursing the loads more accurately models the behavior that is observed in an experiment, as the load cells in an experiment have some amount of surface area in contact with the shells and thus naturally disburse the forces.

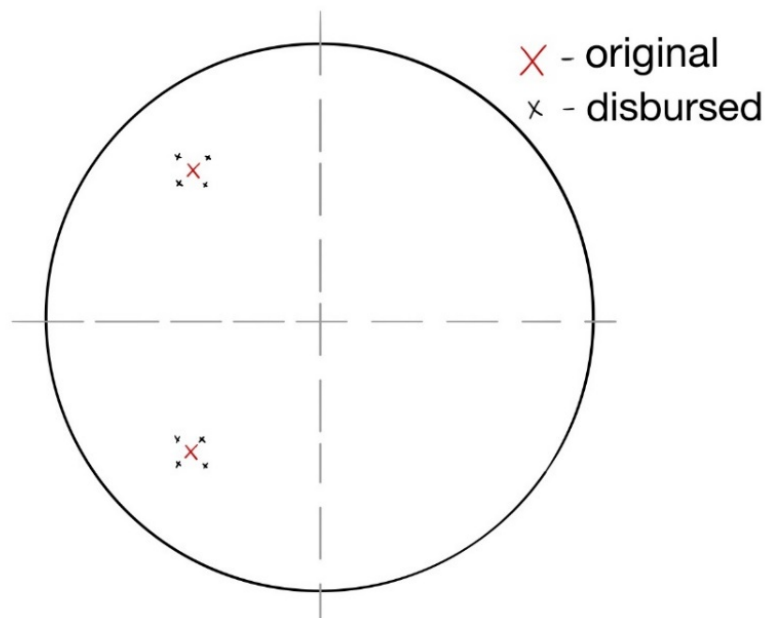


Figure 3.9 – Disbursed vertical loads around two theoretical load points

3.6.2 Secondary Analyses

The secondary analyses refer to the inclusion of more complex information such as material yielding and large deformation effects. Plastic deformation refers to the stage in the load/displacement curve that cannot be reversed by simply unloading the part. The yielding information described in Table 3.3 repeated again below describes the plastic deformation portion of the ABS stress strain curve. If it is found that the failure mode cannot be determined strictly by the primary analysis, then this more detailed analysis is necessary. This study is conducted in Abaqus in three parts. The secondary analyses are run in the static step on each of the shells as described in the flow chart Figure 3.7. The yielding behavior and large deformation behavior are added to each of the hemisphere's models and are loaded to failure individually first. This is to gain an understanding of how each hemisphere looks if it failed purely in buckling and purely in material yielding. Then those two effects are run together and loaded to failure to observe where the combined load/displacement curve mirrors or departs from the two individual behavior curves. This assumes that the most experimentally accurate analysis is the combined results curve, and conclusions are based on that assumption. Results for each of these analyses are tabulated in load/displacement curves for each FEA process. Only the z displacements are taken into account rather than the magnitude of the displacements because there is no force applied in the x or y directions and thus the x and y terms in the strain equation cancel shown in equation 3.7 below. Because there are two load points, the displacements at those points are summed together and tallied with the total force applied.

$$f = u_x F_x + u_y F_y + u_z F_z \quad (3.7)$$

Table 3.3 – Yield behavior values of ABS filament

Yield Data		
Yield Stress (psi)	Yield Stress (MPa)	Plastic Strain
4500	31.0	0
4650	32.1	0.01
4750	32.8	0.02
4800	33.1	0.04
1000	6.9	0.05

4 RESULTS

The results that answer the question stated in the Introduction and stated again below are presented in this chapter.

- Can topology optimization be used to optimize the material placement in a hemisphere?
- Does an optimized hemisphere resist bending and buckling under asymmetric loads better than the classical continuous and grid shell hemisphere geometries?

This thesis calculates the load bearing capacity and failure behavior of the aforementioned three shells. The results are described in three steps. First, the topologically optimized hemisphere geometry is described. Second, the buckling load of each shell was numerically found and those results are verified using existing analytical solutions. Third, the maximum stress induced in each shell by p_{cr} was determined and failure modes are evaluated. Finally, secondary non-linear plastic analyses were conducted on the shells that did not have a determined failure mode from the primary analyses, and the load/displacement curves are discussed to determine failure mode.

4.1 Topology Optimization Results

The problem formulation developed in section 3.5 was used in Abaqus with the Tosca optimizer to discover a novel topology optimized hemisphere shell. The form was optimized under an asymmetrical point loaded condition with two loads applied in the $-z$ direction at the centers of adjacent quadrants depicted in red in Figure 4.1. Dimensions and pin boundary conditions of the optimization domain mirror the dimensions of grid shell that was analyzed in this study and are depicted below in Figure 4.1.

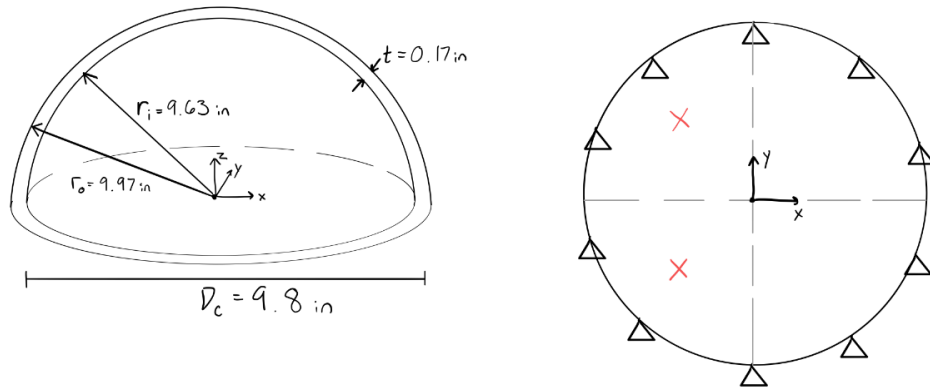


Figure 4.1 – Topology optimized shell domain, with loads and boundary condition drawing

The final topology is depicted in Figure 4.2. The resulting geometry is exported using Rhino and discontinuities were screened for using the built-in Abaqus filtering function. This is done by opening the Job -> Optimization module and selecting export. Five filtering passes are set with default incident angle and stl file output is selected.

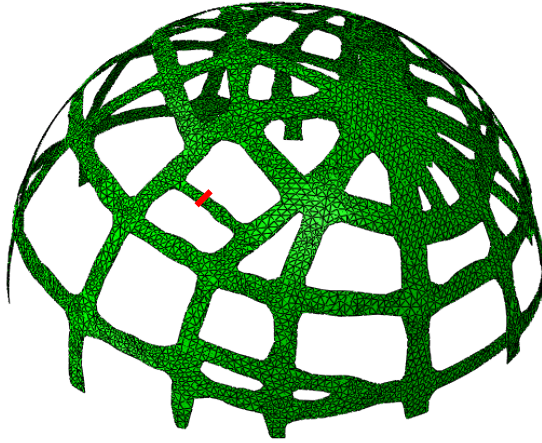


Figure 4.2a – Topology Optimized Hemisphere shell isometric view

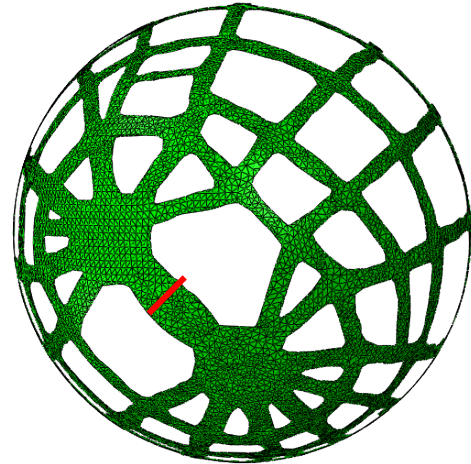


Figure 4.2b – Topology Optimized Hemisphere shell plan view

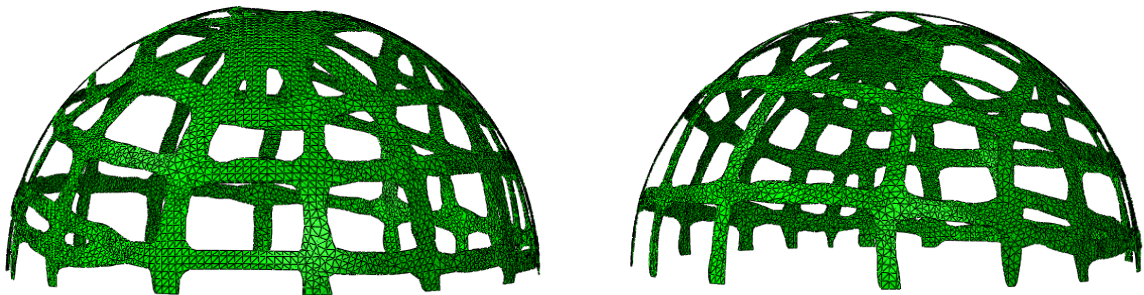


Figure 4.2c -Topology Optimized hemisphere profile views

The topology is similar to the classical grid shell geometry in that it mimics the hoop and meridional members, with the meridional arches spanning from the two load points rather than a single pole. It is expected that material clusters around the two load points due to stress concentrations at those points. All of the members in the optimized shell have a thickness of 0.17", which is identical to the grid shell as defined by the domain. The largest member spans directly between the load points with a width of 0.9" shown in red on Figure 4.2b, while the smallest member has a width of 0.2" shown in red on Figure 4.2a. The spans of the members vary widely, a distinct difference from the grid shell geometry. Near the two poles of the optimized hemisphere the spans average 0.8" - 1.2". The members that are further from the poles tend to span 1.5" - 2.5", which differs from the grid shell shown in Table 4.1.

Table 4.1

Member Dimension	Grid Shell	Opt Shell	
Max Width	0.17	0.9	in
Min Width	0.17	0.2	in
Thickness	0.17	0.17	in
Max Span	2.5	2.6	in
Min Span	1.2	0.8	in
Meridional arches	12	14	
Hoops	6	4	

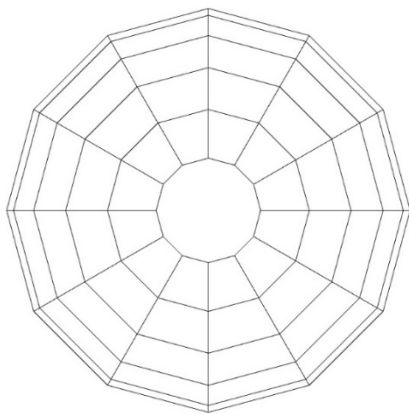


Figure 4.3 – Grid hemisphere plan view

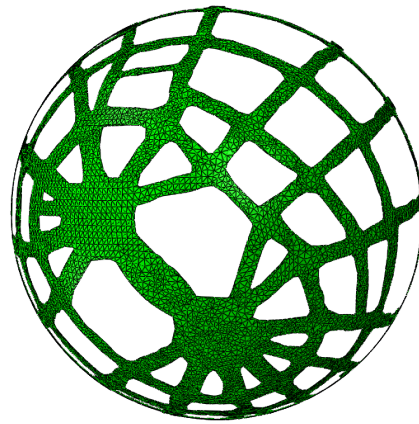


Figure 4.4 – Optimized hemisphere plan view

Plan views of both the grid shell and the optimized shell are shown in Figures 4.3 and 4.4. They are similar in that the meridional arches in both radiate out from specified points. The grid shell has 12 meridional arches and 6 hoop members, while the optimized shell has 8 continuous arches radiating from one of the poles, and 6 from the other, with 4 continuous hoop members.

4.2 Buckling Load Validation

4.2.1 Symmetric Buckling Load Validation

This section describes the validation of the critical buckling load found with Abaqus FEA by using Timoshenko's closed form solution. This is obtained assuming an axisymmetric buckling load, where the radius is defined by R and the Poisson's ratio is ν . This was conducted numerically by completing an eigenvalue analysis of the continuous shell hemisphere in Abaqus. Those results are compared to Timoshenko's solution described in Figure 4.5.

Timoshenko

$$E = 319000 \text{ psi}$$

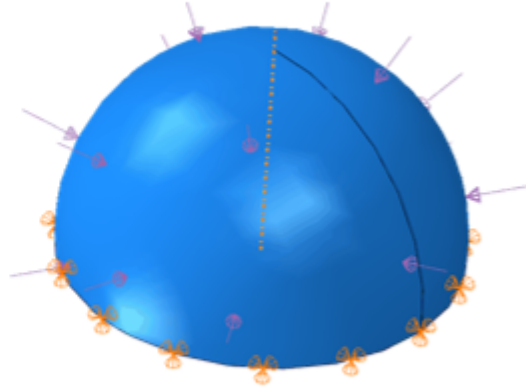
$$\nu = 0.3$$

$$t_{eq} = 0.039 \text{ in}$$

$$R = 4.9 \text{ in}$$

$$p_{cr} = \frac{2E}{\sqrt{3(1-\nu^2)}} \left(\frac{t_{eq}}{R} \right)^2$$

Abaqus



Solution: $p_{cr} = 24.5 \text{ psi}$

$p_{cr} = 25.9 \text{ psi}$

Figure 4.5 – Timoshenko’s closed form solution equation and results, Abaqus FEA numerical solution of critical buckling load analyses

The numerical solution is slightly higher than the theoretical prediction for a continuous shell according to Timoshenko. Numerical solutions are usually stiffer than those found using theoretical continuum methods. In continuum methods there are an infinite number of particles that are free to move in infinite directions. This results in infinite natural frequencies (Malek, 2012). The FEA however only has a predetermined number of natural frequencies governed by the degrees of freedom in the mesh. It is also possible that the mesh size of 0.14" is causing the slightly higher stiffness.

It is also important to note that analytical critical buckling load solutions derived over the past century were found for shallow shells $\frac{L}{h} \geq 6$. These shallow shells transmit forces via membrane action until the bending phase, at which point the behavior changes to snap-through buckling (Malek, 2012). The geometry in this study is a steep shell, where $\frac{L}{h} = 2$, and according to existing literature is governed by bending rather than membrane forces. However this study uses the Timoshenko solution because it is applied to hemisphere shells in literature with consistency (Reis et al., 2020).

4.2.2 Asymmetric Buckling Load Comparison

This section describes the difference between Yamada's asymmetrical critical buckling solution with the numerical solution found in this study (Yamada & Yamada, 1985). Though an *analytical* solution has not been developed for asymmetrically loaded spheres, Yamada developed a unique numerical solution for a *pressure load distributed over half of a spherical cap*. Recall Yamada & Yamada's research, presented in chapter 2, which discovered the critical buckling load decreases by 17-30% when using an asymmetric pressure load distributed over half a spherical cap vs a uniformly distributed pressure load. The free body diagrams depicting Yamada's vs Timoshenko's assumptions are shown in Figure 4.6.

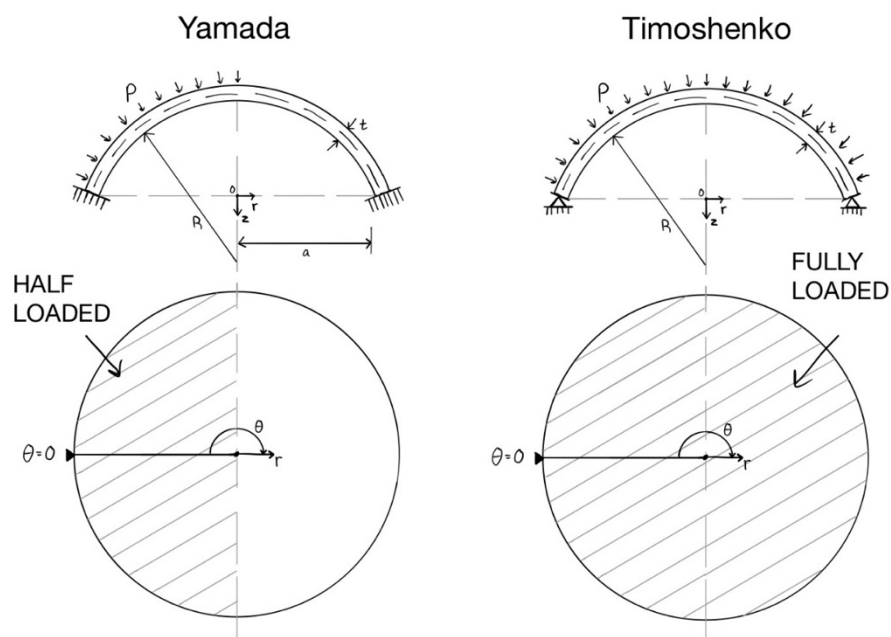


Figure 3.6 - Yamada vs. Timoshenko's boundary conditions and load assumptions

In order to further validate the numerical findings, Yamada's conclusions are measured against the critical buckling load found for an asymmetric pressure load distributed over the continuous hemisphere presented in this study. A pressure load could not be distributed on the face of the grid or optimized shell because the models are made of elements, not faces, and so their irregular geometry lends a pressure load impossible to practically apply. Therefore, only the closed form solutions and Yamada's knockdown predictions for the are shown for all three shells. The results of the pressure critical buckling analyses are shown below in Table 4.2.

Table 4.2 – Timoshenko’s and Yamada’s predictions with numerical solution comparisons

	Continuous	Grid	Optimized	
Timoshenko	24.5	108.4	184.4	psi
FEA Symm p_{cr}	25.9	-	-	psi
Yamada's Asymm Prediction	17.1 – 20.3	75.9 – 90.0	129.1 – 153.1	psi
FEA Asymm p_{cr}	16.8	-	-	psi
Percent Decrease	31%	-	-	%

The differences between Timoshenko and Yamada’s continuum theoretical solutions and the numerical analyses conducted in this study can be partially attributed to the mesh limits in the case of FEA. However, it is shown that the decrease in critical load capacity under an asymmetric distribution holds true as Yamada predicted, only exceeding his prediction by 1%. This short investigation provides validity that the numerical model built in this study reasonably predicts the buckling load of hemispheres. This includes the reduction in buckling capacity under asymmetric versus symmetric load conditions.

4.3 Simple Analysis Results

4.3.1 Elastic Stress Results

This section describes the results of the primary analysis under the two asymmetric point loads as defined in the methodology. The critical buckling load under the asymmetric point loads was found for each hemisphere. The critical loads found by those analyses were then placed back on their respective shells to find the induced stress at the buckling load. The results for each of these are tabulated in Table 4.3 as follows, recall that the ultimate strength of ABS is 4800 psi.

Table 4.3 – Numerical results for buckling load and induced stress by buckling load

	Continuous	Grid	Optimized	
Buckling Load	57	155	908	lbs
Max Stress	1,900	14,000	9,920	psi
Failure Mode	buckling	crushing	crushing	

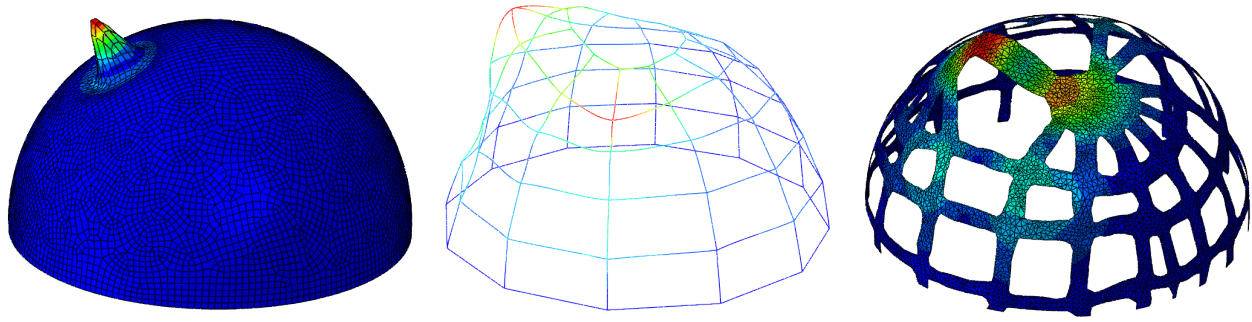


Figure 4.7 - Eigenmode 1 for each of the three hemispheres under asymmetric dual point loads

Figure 4.7 describes the first eigenmode for each shell. Stress results are compared to the 4800psi ultimate strength values published by Stratasys. It is clear that the stress induced by the buckling load of 57lbs on the continuous shell does not nearly approach the strength of ABS plastic. Therefore, the failure mode for the continuous shell is definitively buckling and further plastic analysis is only necessary for the grid and optimized shells.

One thing of note is that the grid shell has a 50% higher maximum stress than the optimized shell, despite being of equal volume and comparable shape. This is potentially due to the amount of material clustered around the load points in the optimized condition. The forces act through a smaller cross section and thus drive up the stress $\sigma = \frac{F}{A}$ in the grid shell. The optimized shell, which has more area where the force is directly applied to the shell, results in a lower maximum stress. It may also have to do with the different discretization's of beam elements vs shell elements. There is also significantly less displacement in the optimized shell than in the grid shell, suggesting that the failure mode of the grid shell is governed by buckling, and the optimized shell is governed by crushing.

4.4 Yielding and Large Deformation Results

This section depicts the results from the secondary analyses on the grid shell and optimized shell. Effects of plastic yielding, nonlinear large deformations, and global failure behaviors are discussed. Results are tabulated in load/deformation graphs and deformations are taken as a sum of the vertical displacements of the two load points.

4.4.1 Plastic and Nonlinear Geometry Effects

Three analyses (large deformation only, yielding only, and combined effects) were done on both the optimized shell and the grid shell. The continuous shell is omitted for this analysis because it was determined from the elastic analysis that the continuous shell fails in buckling, and further investigation is not needed. The elastic-only analysis curves are included to compare the secondary analyses to the primary analyses conducted in section 4.1. The results of the analyses are tabulated in Figure 4.8 below. The combined effects curve is assumed to be the curve that is most like an experiment, so this curve is discussed in the greatest detail. The large deformation and elastic curves are so much longer because there is no upper material-yield limit set in Abaqus for this kind of analysis, so this form can deform much further. The reader should note the different axes of the shells.

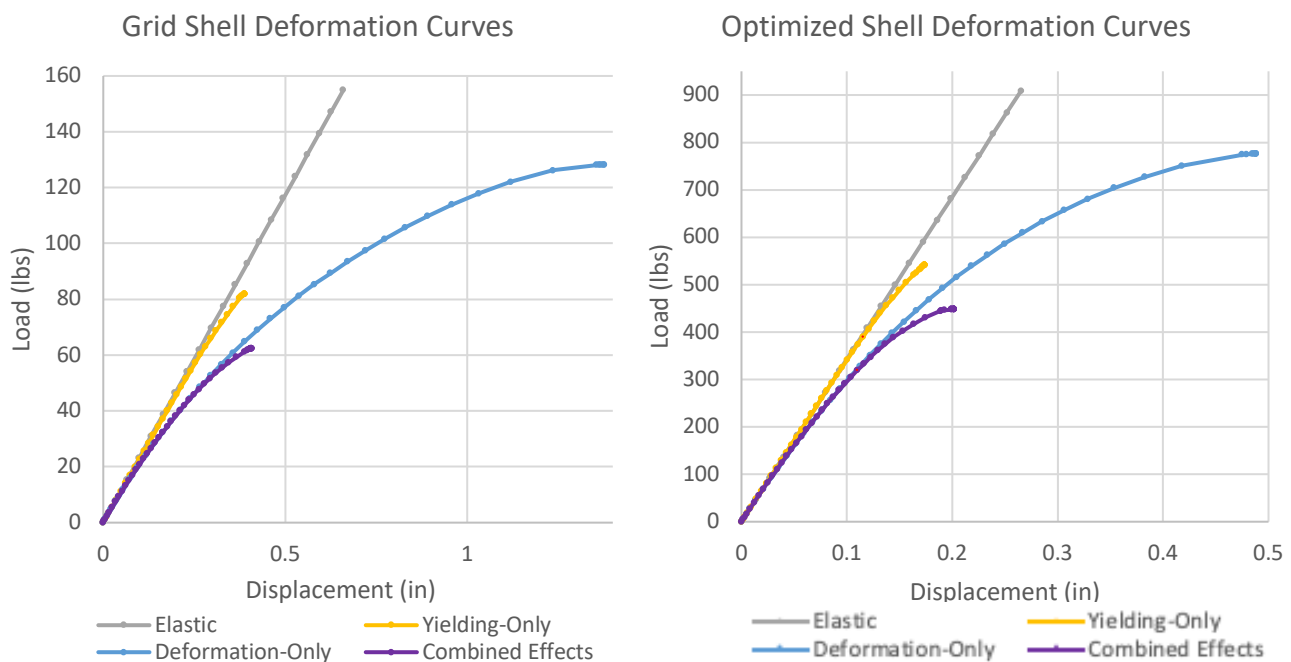


Figure 4.8 - Elastic, Plastic, Large Deformation, and Combined effects Load/Deformation curves for both the grid shell and optimized geometries, under asymmetric point loads

Because the deformation-only and elastic curves are so large and distort the axes, Figure 4.9 below shows the data on a more granular level. In these charts the yield points (plastic strain points) are denoted in red. The yield points are tabulated by inspecting the AC YIELD field output in the Abaqus visualization module and the point at which plastic strain enters the model is recorded.

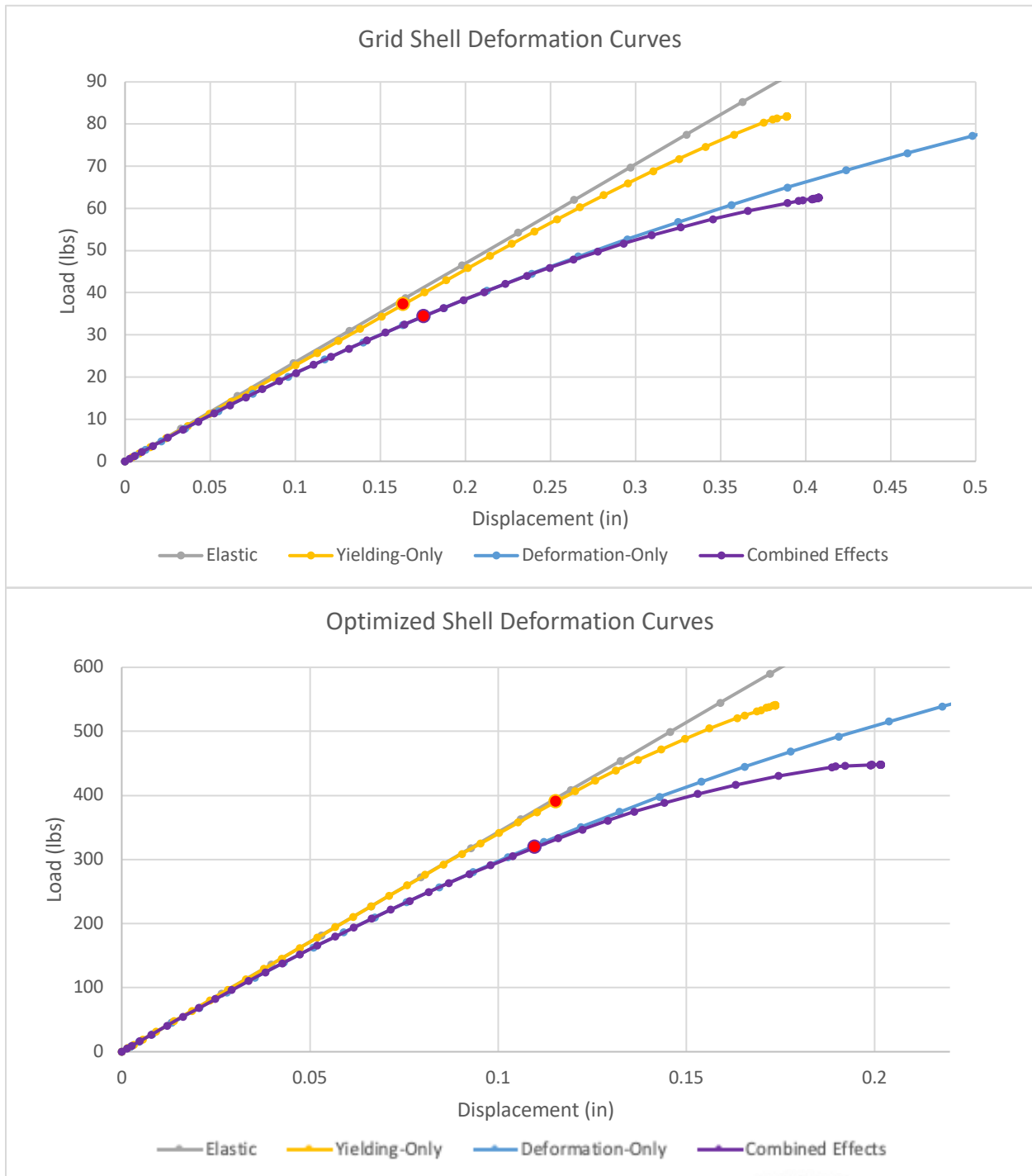


Figure 4.9 - Elastic, Plastic, Large Deformation, and Combined effects Load/Deformation curves for both the grid shell and optimized geometries, under asymmetric point loads. Includes Plastic Strain points

In Figure 4.9 it is clear that the grid shell is governed by deformations because the grid shell combined effects curve follows its deformation-only curve for much longer than the optimized shell does after plastic strain begins. In the optimized shell at the plastic strain point, the combined effects curve immediately deviates from the deformation-only curve. This is the beginning of plastic deformation directly leading to yielding failure. The grid shell begins yielding much earlier in its loading process than the optimized shell, shown by the plastic strain points being closer to the base state. The grid shell's combined effects curve continues to follow the deformation-only curve even after plastic strain, almost until it completely fails. The grid shell end-case minimal deviation from the large deformation curve suggests that yielding does not play as significant a role in failure as in the optimized shells case. Clearly there are combined effects of buckling and yielding in both cases, as the combined effects curves do not follow exactly either the deformation-only curves or the yielding-only curves. However these results indicate that the optimized shell fails in material yielding rather than in buckling. The grid shell being dominated by bending is not surprising as that failure mode is well established in literature (Malek, 2012). The optimized shell geometry is tolerating a very high load without bending through the thickness. This suggests it resists this load via membrane-action forces through the arches and hoops of the hemisphere rather than bending through the thickness as the grid shell does. This alone is a novel discovery: that a simple topological reorganization of material can fundamentally alter the failure behavior of a geometry that was previously believed to act only in bending.

4.4.2 Local vs global behavior

At initial glance, that the grid shell gradually deforms twice what the optimized shell deforms, this would suggest gradual, global buckling. Furthermore, this effect is clearly observed in the two final deformed shapes shown in Figure 4.10. In the optimized shell, deformation is concentrated around the two load points, whereas in the grid shell, almost every member deforms except for the base ring and connected elements. This suggests local yielding is happening in the optimized shell, while global buckling is occurring in the grid shell.

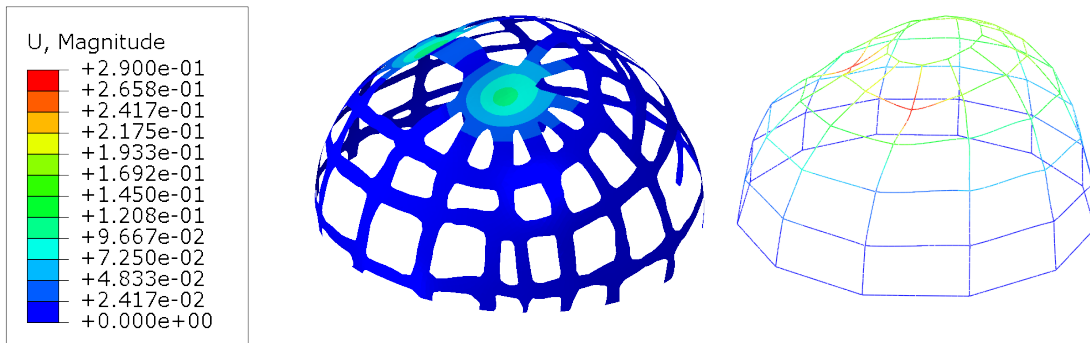


Figure 4.10 - Deformed optimized and grid hemispheres under asymmetric point loads

Recall that the ultimate failure strength of ABS plastic is 4800psi. The optimized shell stress almost reaches this ultimate strength, reaching 4771psi at its final deformed shape. The grid shell on the other hand, while not significantly lower than the ultimate failure stress, comes in 30 psi lower at 4741psi. A comparison of the magnitudes of displacement and maximum stress in each of the shells is provided in Table 4.4.

Table 4.4 – Final displacement and stress at failure

	Grid Shell	Opt Shell	
Displacement	0.41	0.2	in
Stress	4741	4771	psi

This difference is too minimal to definitively draw conclusions. This requires more study and should be modeled with a stronger material to determine if those stress results hold under different material assumptions and finer steps of data.

Figure 4.11 shows the combined effect curves of both shells with plastic strain entrance denoted in red. These results clearly show that the optimized hemisphere is much stiffer than the grid shell configuration, only deforming about half of the amount that the grid shell does, while carrying over six times the load. The gradual and large deformation in the grid shell is evident as well, which further proves its global behavior. The grid shells entire structure is consistently responding to the loads, offering little resistance and instead slowly buckling in a classic elastic, then plastic buckling mode. In contrast the overall stiffness of the optimized shell is so high that the deformation is concentrated around those specific points in a local effect.

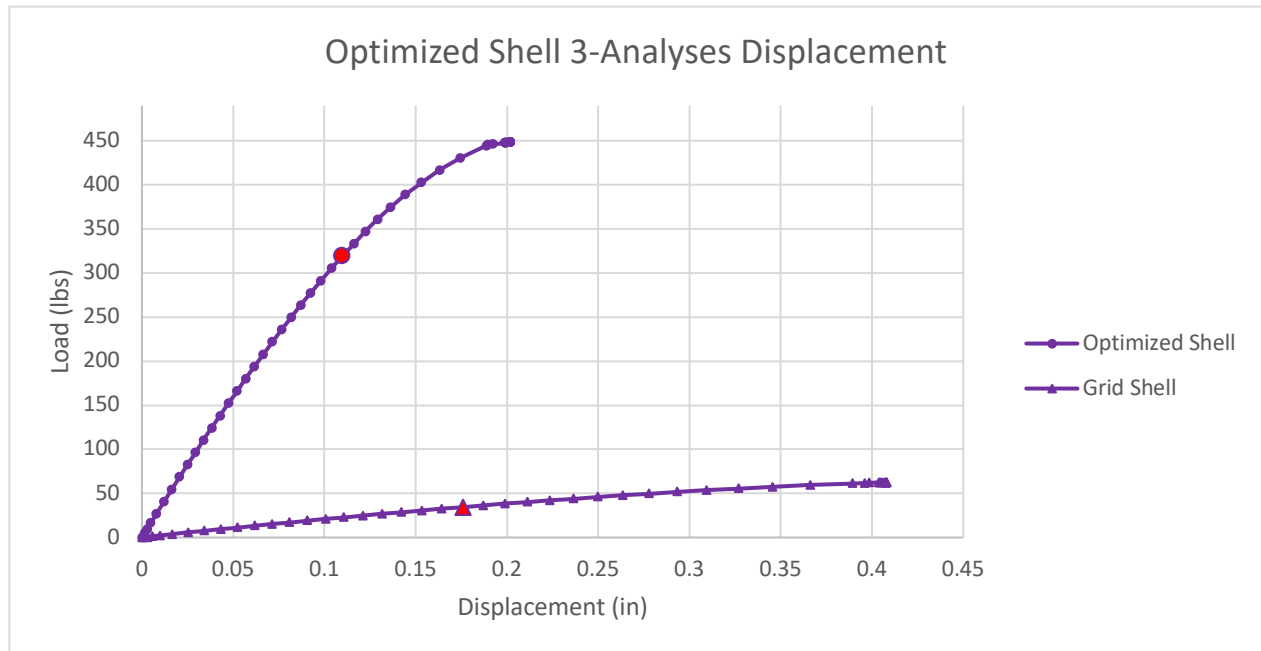


Figure 4.11 - Load vs. displacement of combined effects curves for the grid shell and optimized shell

The large displacement and small deviation from the deformation-only curve in the grid shell shows that it fails in global buckling. On the other hand, the optimized shell, which minimally displaces and clearly deviates from the deformation curve at the point of plastic strain, shows that the optimized shell fails in local material yielding. This is of note because prior to this study, steep shells were undoubtedly governed by bending forces and ultimately buckling failure. This suggests that topology optimization can be applied to steep shells to avoid this buckling failure, and that ultimately the placement of material can fundamentally change shell behavior.

5 CONTRIBUTIONS AND FUTURE WORK

The goals of this thesis were:

- To successfully use topology optimization over a hemisphere shell domain
- To investigate numerically and analytically how the failure mode of a topology optimized shell compares to that of the classic continuous shell and a grid shell
- To provide research for future experimental validation to build upon

These goals were achieved by conducting an analytical and numerical study that investigated the behavior of the three aforementioned hemisphere shells under asymmetric point loads. The results were recorded in load/displacement curves. The stresses and introduction of plastic deformations were discussed to provide a full picture of each shells failure mode. The contributions as a result of this study are summarized in the following section.

5.1 Novel Achievements

This thesis found that topology optimization can be used to develop novel geometries that are stiffer and more resistant to buckling failure than reticulated grid shells. The generation of this optimized hemisphere model was achieved with the FEA software Abaqus, using the Tosca optimizer tool.

To describe the mechanics of this optimized hemisphere, a numerical study was conducted on a continuous shell, grid shell, and this discovered optimized shell. The limits, loads, and boundary conditions were all chosen to mirror possible future experimentation. First, each shells asymmetric point buckling load was discovered numerically. Then elastic analyses were conducted on each of the shells subjected to their own buckling loads. In the secondary analyses, yielding and large deformation effects were introduced. It was found that the continuous hemisphere is clearly governed by local buckling failure in the elastic analysis. In the plastic analysis it was confirmed that the grid shell hemisphere is governed by bending forces resulting in buckling, but results showed that the optimized shell is governed by membrane forces, translating to a more material yielding failure mode. This is significant for two reasons. The first is that a spherical shell cap has never been optimized using the topological method. The second is that literature describes steep shells as unequivocally governed by bending and buckling. The findings in this thesis challenge that notion and indicate this could be a viable method to design stronger shells.

This method could potentially be used in the future for a number of applications that extend beyond the conventional domains that use topology optimization. Considering one innovation of this thesis is intricately constraining the optimization domain, many more problems that face specific geometric constraints could be explored. Specifically with shells, this method could be used to design shells that are more complicated in curvature and geometry.

5.2 Shell Module for other loads

In reality, asymmetric loads on structures are more accurately represented by lateral wind loads or drifted snow loads rather than point loads as analyzed in this thesis. The building code enumerates many asymmetric loading conditions that do not follow the dual point loaded hemisphere that is created in this study. However, there is potential for this process to be used to modularize a section of a hemisphere that could then be repeated periodically around the circumference of the geometry either as a standalone grid shell or via some system of reinforcement. An optimization of 1/6th of a hemisphere under a single point load was done to illustrate this point and is shown below in Figure 6.1.

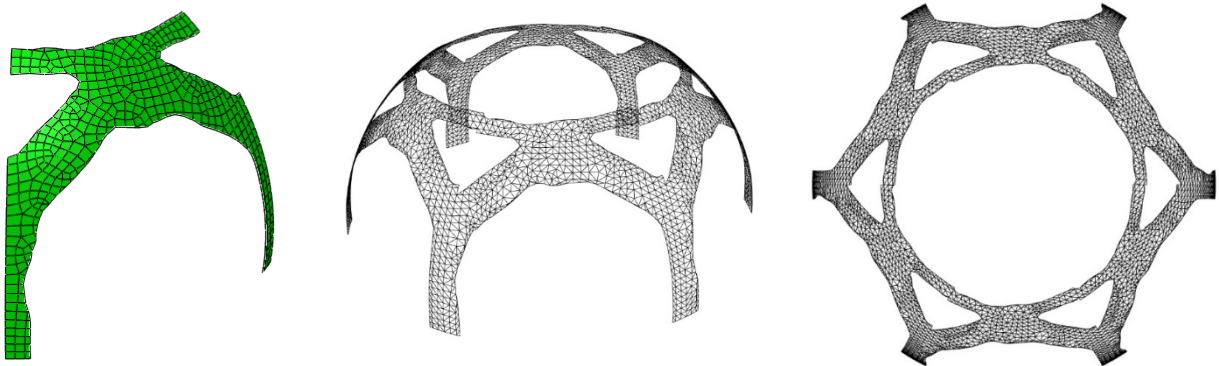


Figure 4.1 - Topology Optimized rotatable module under a single point load, then rotated periodically to create a full hemisphere

The green mesh is the optimized Abaqus module under a single vertical point load. Once this was completed the topology was extracted to Rhino and repeated periodically to create a full hemisphere. This is not an unfamiliar shape and mimics some existing arched domes with oculi. However, this was only optimized using this singular load case. Different results would be captured using different constraints and different load cases. To design a structure that could resist more load cases it could either be optimized for multiple load cases or revolve a different section size. It is also noted that there was no hole size constraint placed on this hemisphere. In reality, much more material would need to be added to close

the oculus in the center of the form. However, this could be achieved as well as many different goals by adding constraints that fit the users preferences.

5.3 Discussion

5.3.1 Optimization: Maximizing Buckling Load

When discussing optimization, there is a question of what objective to optimize. The objective of this study was to minimize compliance. The possibility of an objective to maximize the buckling load was considered, however eigenfrequency is notoriously erratic and rarely converges (Bruyneel et al., 2008). This was attempted for this study at first however the general rule of nonconvergence took precedence over the strain energy constraints placed on the shell to try and encourage this convergence. Sigmund and Ferrari successfully completed an eigenvalue optimization by investigating different lower bounds on the critical load. However in order to achieve this they use non-conforming finite elements, inconsistent sensitivities, and replaced single eigenvalue constraints with an aggregated measure (Ferrari & Sigmund, 2019). This is an interesting route for future research as this study was among the first of its kind. The field would benefit from further research into this area and would have some similarities. The shell domain mimics the 2D domain over which Sigmund and Ferrari's analysis was conducted, as the shell is simply a 2D surface bent into the 3rd dimension.

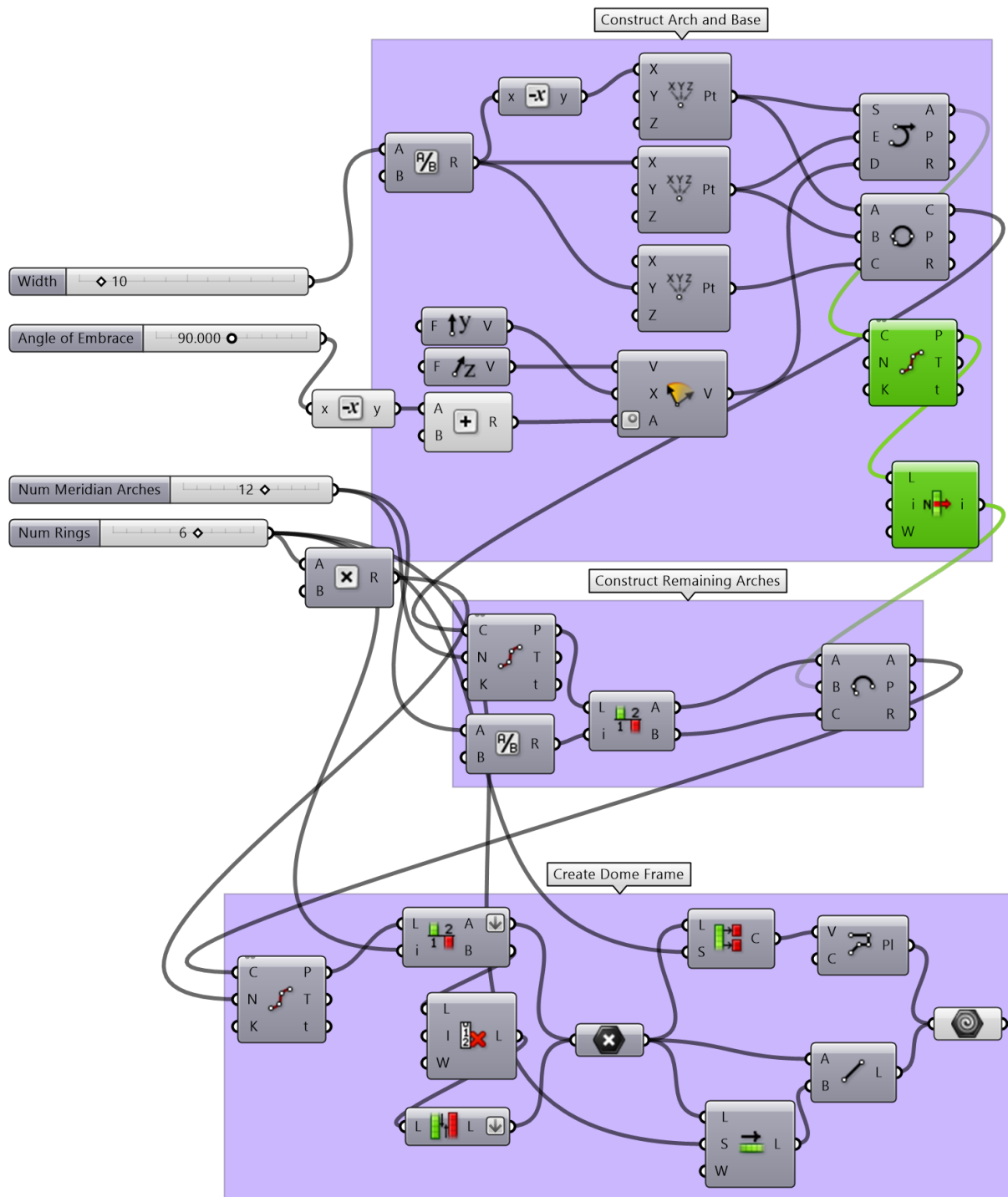
5.3.2 Potential for Experimentation

Originally this study meant to explore the results of an experimental process. Unfortunately due to the Coronavirus crisis this was rendered impossible. The decisions about sizing, material, loading, and boundary conditions were based on the plan to carry out an experiment, and the methodology provides a step-by-step process to conduct an experiment on these shells with justifications for each methodological choice. The field would benefit from an experimental analysis conducted on a topology optimized shell structure to deepen the understanding of these results. This is specifically because it is likely that in reality the load capacity of the optimized hemisphere is exaggerated in this numerical analysis. The shape in this thesis was a three dimensioned shape but analyzed as an idealized two dimensional shell lofted into the third dimension. Therefore, it is likely that during experimentation the difference in the load capacity of the optimized versus classic hemispheres load will be less severe.

5.3.3 Effects of Anisotropy

Because this study was initially conducted with the purpose of experimentation, the effects that the FDM would have had on the behavior of the model cannot be ignored. The discontinuities of printing would significantly lower the failure load. As previously discussed, Mark Tam and Frank Fang both conducted studies on the effects of anisotropy on the mechanics of printed parts (Fang, 2017; Tam, 2015). Fang found that the actual strength values and strain percentages were significantly lower than the Stratasys published values. This could be a result of the superior printing equipment used by Stratasys, likely with much higher printing precision than a Stratasys F170. Mark Tam investigated the effects of printing orientation specifically on a shell. Rather than print conventionally, he calculated the stress lines of a shell under an apex point loading and then wrote a script to condense and convert them to tool paths. Then he printed filament along those stress lines. If the author had been able to conduct experimentation as initially hoped, it is likely that the hemispheres would have failed sooner than computationally predicted. This challenges the results as accurate predictors of physical load capacities, but retains the intent as a tool for comparison between the shells, and so served the purpose of this study. A more accurate prediction could be achieved if Fangs discovered values for yield strength, ultimate strength, and strain percentages were used rather than the Stratasys values. Anisotropy is notoriously difficult to model due to discrepancies in layer height, print speed, and infill orientations, and so were outside the scope of this thesis. However investigating the possibility of accurately modelling anisotropy could be a viable and useful path for future work.

Appendix A



6 BIBLIOGRAPHY

- Abaqus/CAE User's Guide*. (2016). <http://130.149.89.49:2080/v2016/books/usi/default.htm>
- AD Classics: Kresge Auditorium / Eero Saarinen and Associates*. (2014, April 3). ArchDaily. <http://www.archdaily.com/492176/ad-classics-kresge-auditorium-eero-saarinen-and-associates/>
- Adriaenssens, S., Tysmans, T., Cuypers, H., & Wastiels, J. (2009). Structural analysis of small span textile reinforced concrete shells with double curvature. *Composites Science and Technology*, 69(11), 1790–1796. <https://doi.org/10.1016/j.compscitech.2008.09.021>
- Al-Rashed, R., López Jiménez, F., Marthelot, J., & Reis, P. M. (2017). Buckling patterns in biaxially pre-stretched bilayer shells: Wrinkles, creases, folds and fracture-like ridges. *Soft Matter*, 13(43), 7969–7978. <https://doi.org/10.1039/C7SM01828B>
- Baek, C., & Reis, P. M. (2019). Rigidity of hemispherical elastic gridshells under point load indentation. *Journal of the Mechanics and Physics of Solids*, 124, 411–426. <https://doi.org/10.1016/j.jmps.2018.11.002>
- Bălut, N., & Gioncu, V. (2000). The Influence of Geometrical Tolerances on the Behaviour of Space Structures. *International Journal of Space Structures*, 15(3), 189.
- Bendsøe, M. (1989). Optimal shape design as a material distribution problem. *Structural Optimization*, 1(4), 193.
- Bendsøe, M. P., & Sigmund, O. (1999). Material interpolation schemes in topology optimization. *Archive of Applied Mechanics*, 69(9), 635–654. <https://doi.org/10.1007/s004190050248>
- Bendsøe, Martin P., & Sigmund, O. (2003). Topology, optimization: Theory, methods, and applications. In *Topology, optimization: Theory, methods, and applications / M.P. Bendsøe, O. Sigmund*. <https://lib.mit.edu/record/cat00916a/mit.001133782>
- Bendsøe, Martin Philip, & Kikuchi, N. (1988). Generating optimal topologies in structural design using a homogenization method. *Computer Methods in Applied Mechanics and Engineering*, 71(2), 197–224. [https://doi.org/10.1016/0045-7825\(88\)90086-2](https://doi.org/10.1016/0045-7825(88)90086-2)
- Berman, F. R. (1946). *Mathematical analysis of stress and displacement in thin shallow spherical shells* [Thesis, Massachusetts Institute of Technology]. <https://dspace.mit.edu/handle/1721.1/12772>
- Borezo, A., & Fuller, R. B. (2010). Raising the supine dome. In *Raising the supine dome / [by Amy Borezo]*. <https://lib.mit.edu/record/cat00916a/mit.002611217>
- Bruyneel, M., Colson, B., & Remouchamps, A. (2008). Discussion on some convergence problems in buckling optimisation. *Structural and Multidisciplinary Optimization*, 35(2), 181–186. <https://doi.org/10.1007/s00158-007-0129-z>
- DeJong, M. J. (Matthew J. (2009). *Seismic assessment strategies for masonry structures* [Thesis, Massachusetts Institute of Technology]. <https://dspace.mit.edu/handle/1721.1/49538>
- Fang, F. Y. (2017). *Effect of print orientation on mechanical material behavior in fused deposition modeling 3-D printing* [Thesis, Massachusetts Institute of Technology]. <https://dspace.mit.edu/handle/1721.1/111505>
- Ferrari, F., & Sigmund, O. (2019). Revisiting topology optimization with buckling constraints. *Structural & Multidisciplinary Optimization*, 59(5), 1401–1415. <https://doi.org/10.1007/s00158-019-02253-3>
- Geckeler, J. W. (1926). *Über die Festigkeit Achsen-symmetrischer Schalen*. Forsch-Arb. Ingwes.
- Gioncu, V. (1985). Instability Problems in Space Structures. *International Journal of Space Structures*, 1(3), 169.

- Gioncu, V. (1995). Buckling of Reticulated Shells: State-of-the-Art. *International Journal of Space Structures*, 10(1), 1.
- Hassani, B., Tavakkoli, S. M., & Ghasemnejad, H. (2013). Simultaneous shape and topology optimization of shell structures. *Structural and Multidisciplinary Optimization*, 48(1), 221–233. <https://doi.org/10.1007/s00158-013-0894-9>
- Hutchinson, J. W., Marthelot, J., López Jiménez, F., Lee, A., & Reis, P. M. (2017). Buckling of a Pressurized Hemispherical Shell Subjected to a Probing Force. *Journal of Applied Mechanics*, 84(12). <https://doi.org/10.1115/1.4038063>
- Kollár, L., & Dulácska, E. (1984). Buckling of shells for engineers. In *Buckling of shells for engineers / L. Kollár and E. Dulácska*. <https://lib.mit.edu/record/cat00916a/mit.000197371>
- Kovářík, M., michal.kovarik@fsv.cvut.cz, Svoboda, P., pavel.svoboda@fsv.cvut.cz, & Achten, H. H., achten@fa.cvut.cz. (2019). Limits and Potential of 3D Printing Technologies for Construction of Concrete Shells. *Solid State Phenomena*, 292, 249–256. <https://doi.org/10.4028/www.scientific.net/SSP.292.249>
- Kuznetsov, V., Solonin, A., Urzhumtsev, O., Schilling, R., & Tavitov, A. (2018). Strength of PLA Components Fabricated with Fused Deposition Technology Using a Desktop 3D Printer as a Function of Geometrical Parameters of the Process. *Polymers*, 10(3), 313. <https://doi.org/10.3390/polym10030313>
- Lefevre, B., Douthe, C., & Baverel, O. (2015, September). *Buckling of Elastic Gridshells* [Text]. International Association for Shell and Spatial Structures (IASS). <https://www.ingentaconnect.com/search/article?option1=tk&value1=Buckling+of+Elastic+Gridshells&pageSize=10&index=1>
- López, A., Puente, I., & Serna, M. A. (2007). Numerical model and experimental tests on single-layer latticed domes with semi-rigid joints. *Computers & Structures*, 85(7), 360–374. <https://doi.org/10.1016/j.compstruc.2006.11.025>
- Mainstone, R. J. (1975). *Developments in structural form* (Library Storage Annex - Off Campus Collection TH145.M2796 1975b). Cambridge, Mass. : M.I.T. Press, 1975.
- Malek, S. R. (Samar R. (2012). *The effect of geometry and topology on the mechanics of grid shells* [Thesis, Massachusetts Institute of Technology]. <https://dspace.mit.edu/handle/1721.1/74425>
- Meissner, E. (1915). *Über Elastizität und Festigkeit dünner Schalen* (Vol. 60). Vierteljahrsschrift der Naturforschenden Gesellschaft.
- Mesnil, R., & Engineering, M. I. of T. D. of C. and E. (2013). *Stability of elastic grid shells*. [EBook]. Stability of Elastic Grid Shells / by Romain Mesnil. <https://lib.mit.edu/record/cat00916a/mit.002172671>
- Mesnil, R., Ochsendorf, J., & Douthe, C. (2015). Stability of Pseudo-Funicular Elastic Grid Shells. *International Journal of Space Structures*, 30(1), 27–36. <https://doi.org/10.1260/0266-3511.30.1.27>
- Milazzo, M., Muyshondt, P. G. G., Carstensen, J., Dirckx, J. J. J., Danti, S., & Buehler, M. J. (2020). *De novo topology optimization of Total Ossicular Replacement Prostheses*. <https://doi.org/10.1016/j.jmbbm.2019.103541>
- Molke, E. C., & Kalinka, J. E. (1938). Principles of Concrete Shell Dome Design. *Journal of the American Concrete Institute*, 34, 649.
- Nasto, A., & Reis, P. M. (2014). Localized Structures in Indented Shells: A Numerical Investigation. *Journal of Applied Mechanics*, 81(12), 121008. <https://doi.org/10.1115/1.4028804>
- Otto, F., & Rasch, B. (1996). *Finding Form: Towards an Architecture of the Minimal*. Edition Axel Menges GmbH.
- Paoli, C. (Céline A. (2007). *Past and future of grid shell structures* [Thesis, Massachusetts Institute of Technology]. <https://dspace.mit.edu/handle/1721.1/39277>

- Pasternak, P. (1926). *Die Praktische Berechnung Biegeester Kugelschalen, Kreisrunder Fundamentplatten auf elastischer Bettung and Kreissylindrischer Wandungen in gegenseitiger monolither Verbindung* (Vol. 6). Zeitschrift für Angewandte Mathematik und Mechanik.
- Reis, P. M., Yan, D., & Pezzulla, M. (2020). Buckling of pressurized spherical shells containing a through-thickness defect. *Journal of the Mechanics and Physics of Solids*, 138, 103923. <https://doi.org/10.1016/j.jmps.2020.103923>
- Reissner, E. (1946). Stresses and small displacements of shallow spherical shells. II. *Journal of Mathematics and Physics. Massachusetts Institute of Technology*, 25(25), 279.
- Rhinoceros User's Guide—Introduction*. (n.d.). Retrieved May 4, 2020, from <http://docs.mcneel.com/rhino/6/usersguide/en-us/index.htm>
- Schwerin, E. (1919). *Über Spannungen in Symmetrisch and Unsymmetrisch Belasteten Kugelschalen (Kuppeln) insbesondere bei Belastung durch Winddruck* (Vol. 12). Armierter Beton.
- Smith, E. B. (1971). *The dome; a study in the history of ideas* (Rotch Library - Stacks NA2890.S646 1971). Princeton, N.J., Princeton University Press, [1971,c1950].
- Stromberg, L. L., Beghini, A., Baker, W. F., & Paulino, G. H. (2011). Application of layout and topology optimization using pattern gradation for the conceptual design of buildings. *Structural and Multidisciplinary Optimization*, 43(2), 165–180. <https://doi.org/10.1007/s00158-010-0563-1>
- Stromberg, L. L., Beghini, A., Baker, W. F., & Paulino, G. H. (2012). Topology optimization for braced frames: Combining continuum and beam/column elements. *Engineering Structures*, 37, 106–124. <https://doi.org/10.1016/j.engstruct.2011.12.034>
- Tam, K.-M. M. (2015). *Principal stress line computation for discrete topology design* [Thesis, Massachusetts Institute of Technology]. <https://dspace.mit.edu/handle/1721.1/99630>
- Timoshenko, S., & Gere, J. M. (1961). *Theory of elastic stability*. [Electronic resource]. Mineola, N.Y. : Dover Publications, 2009.
- Vantyghem, G., De Corte, W., Shakour, E., & Amir, O. (2020). 3D printing of a post-tensioned concrete girder designed by topology optimization. *Automation in Construction*, 112, 103084. <https://doi.org/10.1016/j.autcon.2020.103084>
- Vaulot, L. K.-L. (2016). *Form-finding of elastic gridshells* [Thesis, Massachusetts Institute of Technology]. <https://dspace.mit.edu/handle/1721.1/104247>
- Wright, D. T. (1966). Membrane forces and buckling in reticulated shells. *Reply*, 92, 401–407.
- Xia, Y., Wu, Y., & Hendriks, M. A. N. (2019). Simultaneous optimization of shape and topology of free-form shells based on uniform parameterization model. *Automation in Construction*, 102, 148–159. <https://doi.org/10.1016/j.autcon.2019.02.018>
- Yamada, S., & Yamada, M. (1985). Buckling and postbuckling behavior of half-loaded shallow spherical shells. *International Journal of Non-Linear Mechanics*, 20(4), 239–248. [https://doi.org/10.1016/0020-7462\(85\)90032-0](https://doi.org/10.1016/0020-7462(85)90032-0)